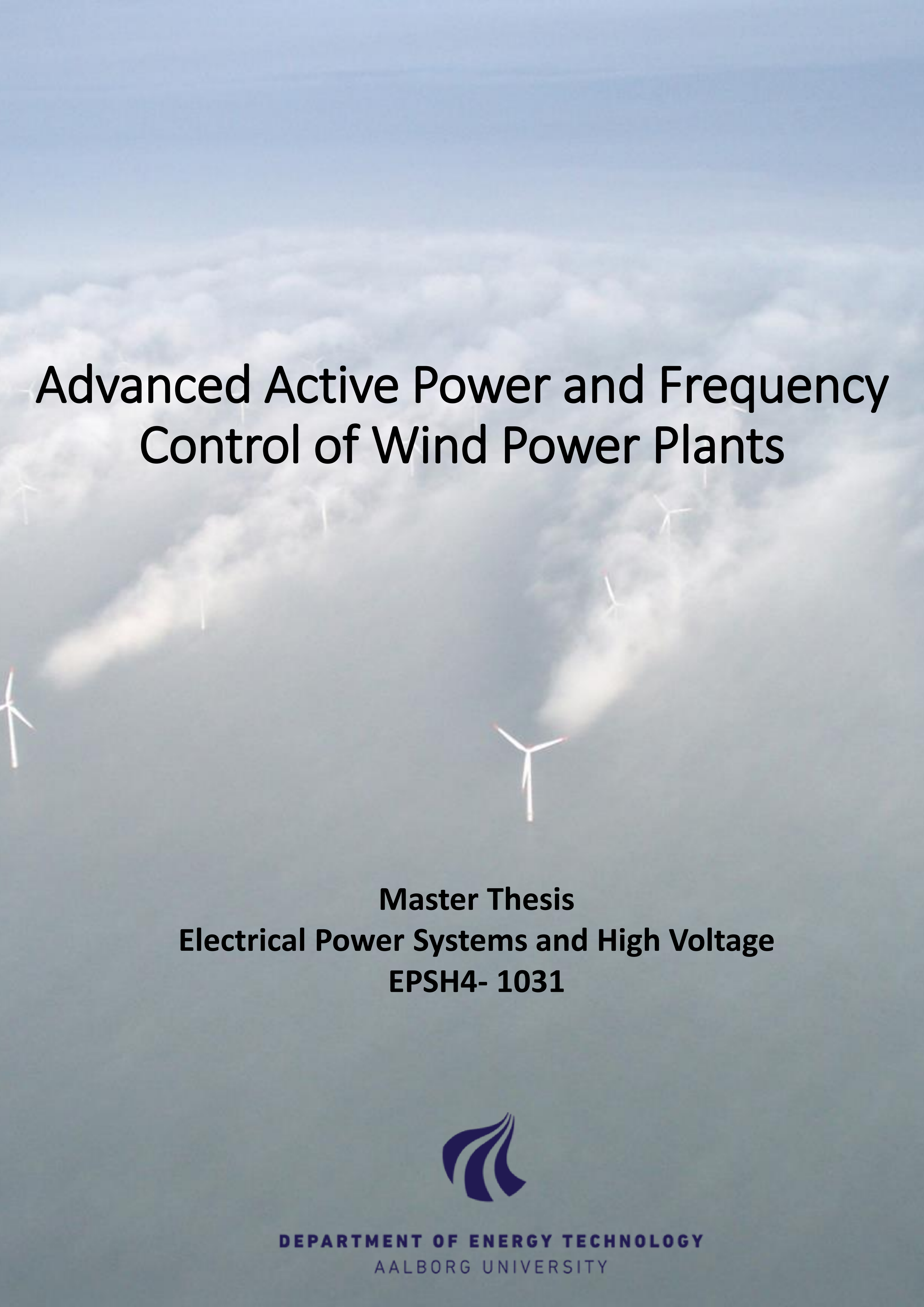

Advanced Active Power and Frequency Control of Wind Power Plants

Master Thesis
Electrical Power Systems and High Voltage
EPSH4- 1031

DEPARTMENT OF ENERGY TECHNOLOGY
AALBORG UNIVERSITY

Title:	Advanced Active Power and Frequency Control of Wind Power Plants
Semester:	10
Semester theme:	Master Thesis
Project period:	01.02.2017 to 01.06.2017
ECTS:	30
Supervisors:	Florin Iov
Project group:	EPSH4 - 1031

Claudiu Ionita

Copies: 5
No. of pages: 61
No. of appendixes : 0
Finished: 01-06-2017

Synopsis:

This project deals with the design and tuning of a wind farm controller, with focus on the active power and frequency control. A model of a 160 MW wind farm, containing 80 wind turbines is implemented to verify the controller functionalities. The requirements of the controller are based on the Danish grid codes.
A PI-controller has been designed using the Modulus Optimum criteria and implemented into a main controller. The robustness of the controller and disturbance rejection capability has been verified successfully for different operating conditions. Two dispatch methods are investigated: equal and proportional to the available power. The latter is chosen due to its superior performance.
The impact of the controller sampling time and discretization method on the performance is investigated both in an offline simulation and in a Real-Time environment using OPAL-RT.
The outcome of this project is a stepwise method to design and tune the active power controller.

The content of this report is public.
By signing this document all group members confirm that everyone has participated equally in the project and that everyone is equally responsible for the content of this report. Furthermore all group members are liable for that plagiarism does not exist in this report.

Preface

The work on this project has been carried out by group EPSH4-1031 at Aalborg University as a part of the Master Thesis in *Electrical Power Systems and High Voltage*. The theme of the project is *Advanced Active Power and Frequency Control of Wind Power Plants*. Prerequisites for reading the report is basic knowledge regarding electrical power systems and control theory. The project deals with designing a control structure, which is able to regulate the active power of a WF to fulfil the Danish grid codes and to provide grid support in case of frequency deviations.
The author would like to thank the main supervisor, Associate Professor Florin Iov for the help and guidance offered through out the project. The author would also like to thank Alin George Raducu, from Vattenfall for support, project proposal, data provided and for the workshop held at the company.

Reading guide

Figures and tables in the report are numbered according to the respective chapter. In this way the first figure in chapter 3 has number 3.1, the second number 3.2 and so on. Explanatory text is found under the given figures and tables. Figures without references are made by the author.

Claudiu Ionita

Summary

The work presented in this report originates in a project proposal from Vattenfall, which has an ambition to develop their own Wind Farm Controller (WFC). A WFC can be divided into two main research areas, active power/frequency control and reactive power/voltage control. The part dealing with the voltage control control has been treated by another group of students. It is therefore chosen to deal only with the active power control in this thesis.

The report is divided in 8 major chapters and their content will be briefly discussed in this summary. The motivation for carrying out the project is stated in Chapter 1. In addition to that, the objectives are stated clearly together with the limitations, which are imposed due to time constraints.

The state of the art regarding WFC is presented in Chapter 2. A review of the scientific literature, which deals with the topic of active power control in WFs is made. The only control structure, which has been proven to work in an actual WF is based on a main controller, which uses a PI to regulate the power in the Point of Common Coupling (PCC). This is therefore the control architecture chosen for this project. Different optimization techniques, such as structural fatigue reduction, reduction of active power losses, etc. have been proven theoretically, but there has not been done a validation for any of them.

In Chapter 3 the modelling of the major grid components is presented. For the cables a lumped π-model is used. The external grid, which is managed by the TSO, is modelled using the Thevenin equivalent. The grid impedances are calculated based on the SCR and XR of the grid. The wind turbines are modelled as current sources.

A model is developed in Simulink and is verified against a power systems simulation tool. The difference in the bus voltages is maximum 0.3 % and the difference in the total active power losses in the grid is maximum 1.61 %. Since the developed model has an acceptable accuracy, a series of simulations have been performed to investigate the influence of different parameters such as SCR, XR, external grid voltage, loading and power factor on the active power losses. The results are presented in Chapter 4, together with a method to obtain a simplified plant transfer function.

Chapter 5 contains the design and tuning of the controller, which is based on requirements imposed by the Danish grid codes. The robustness of the controller is successfully verified for different scenarios and operating conditions.

The impact of discretization method and sampling time on the robustness and performance of the controller is analysed in Chapter 6. In addition to that, the model is implemented and run successfully in a Real-Time environment.

Chapter 7 contains the conclusion and Chapter 8 contains a short description of the future work to be done.

Nomenclature

Symbol	Specification	Unit
B	Susceptance	[S]
C	Capacitance	[F]
K	Tuning gain	[-]
K_P	Proportional gain	[-]
K_R	Integrator reset gain	[-]
K_I	Integral gain	[-]
R	Resistance	[Ω]
I	Current	[A]
L	Inductance	[H]
P	Active power	[W]
$P_{WT,i}^{ref}$	Power reference of the i'th wind turbine	[p.u.]
P_{WF}^{av}	Total available power of the WF	[p.u.]
P_{WF}^{ref}	Reference power sent to the WF	[p.u.]
P_{WF}^{rated}	Rated power of the WF	[p.u.]
P_{WF}^{loss}	Active power losses of the WF grid	[p.u.]
P_{TSO}^{ref}	Active power reference set by the TSO	[p.u.]
P_{PCC}^{ref}	Active power reference in the PCC	[p.u.]
P_{PCC}^{meas}	Measured active power in the PCC	[p.u.]
P_{PCC}^{out}	Actual active power in the PCC	[p.u.]
Q	Reactive power	[W]
s	Droop	[%]
t	Time	[s]
T_s	Sampling time	[s]
τ	Time constant	[s]
v	Wind velocity	[$\frac{m}{s}$]
V	Voltage	[V]
X	Reactance	[Ω]
Y	Admittance	[S]
Z	Impedance	[Ω]

Acronyms

Acronym	Specification
DFIG	Doubly Fed Induction Generator
EWEA	European Wind Energy Association
FSC	Full Scale converter
GUI	Graphical User Interface
HIL	Hardware in the Loop
MPPT	Maximum Power Point Tracking
PFI	Power Fluctuating Index
PoC	Point of Connection
PCC	Point of Common Coupling
RES	Renewable Energy Source
RT	Real Time
SCR	Short-circuit Ratio
SISO	Single Input Single Output
STATCOM	Static Synchronous Compensator
TSO	Transmission System Operator
VSC	Voltage Source Converter
WF	Wind Farm
WFC	Wind Farm Controller
WPP	Wind Power Plant
WT	Wind Turbine

Table of contents

Introduction 1

1.1 Background of the Wind Farm Controller

Conventional power plants, which run on fossil fuels are being replaced by renewable energy sources (RES) at an increasing rate. The role and control capabilities of the synchronous generation units needs therefore to be taken by the new renewable plants. The installation of offshore wind turbines is on the rise, while the area suitable for installing onshore wind turbines(WTs) is diminishing. According to a report provided by the European Wind Energy Association (EWEA), in Europe alone ,there have been installed wind turbines with a total power of more than 3000 MW in 2015 [1]. However, the intermittent nature of the wind and the technology used to transfer the generated power into the grid pose some challenges related to the quality of the power produced, which can lead to voltage fluctuations, harmonics, etc. The majority of the offshore wind turbines are clustered into wind farms, which have different behaviour during dynamic and transient periods compared to single wind turbines. Since the share of wind farms into the electricity grid is increasing, it is more important to understand how the wind farms affect and can contribute to the stability of the grid. It is therefore crucial to develop control strategies that accurately control the active and reactive power in the point of common coupling (PCC). Research focusing on reactive power and voltage control functions is widely encountered in the literature [2] [3]. On the other side the active power is more challenging due to the intermittent nature of the RES and it has far more reaching consequences, being directly related to the frequency stability [4].

The typical layout of a wind farm can be seen in Figure 1.1. The individual wind turbines are clustered in feeders and the resulting current is summed into the collector bus. The voltage is boosted by transformer TR1. Depending on the distance to the onshore connection the power is transferred either by an AC or DC connection (DC connections are usually used when the distance to the onshore connection point is long). Then the voltage is increased even more by the transformer TR2 and the connection to the transmission lines is made. In the PCC, there is typically also installed a STATCOM to provide reactive power compensation, because it is not efficient to transfer reactive power on long distances.

The wind farm (wind power plant) is treated as a single generation unit, so the control of the wind farm is made in the PCC to obtain a behaviour similar to a conventional power plant. A hierarchical control structure is utilized, where a main wind farm controller (WFC) receives the control parameters and the desired set-points either from the Transmission System Operator (TSO) or from the WF operator. The WFC has to ensure that the setpoints are tracked accurately and must make decisions based on the state of the system (i.e. current wind conditions at each WT, voltage, etc.). In order to achieve this a communication infrastructure exists between the PCC, WTs and the WFC, where different measurements (e.g. frequency, voltage level, active, reactive power, etc.) and setpoints are exchanged.

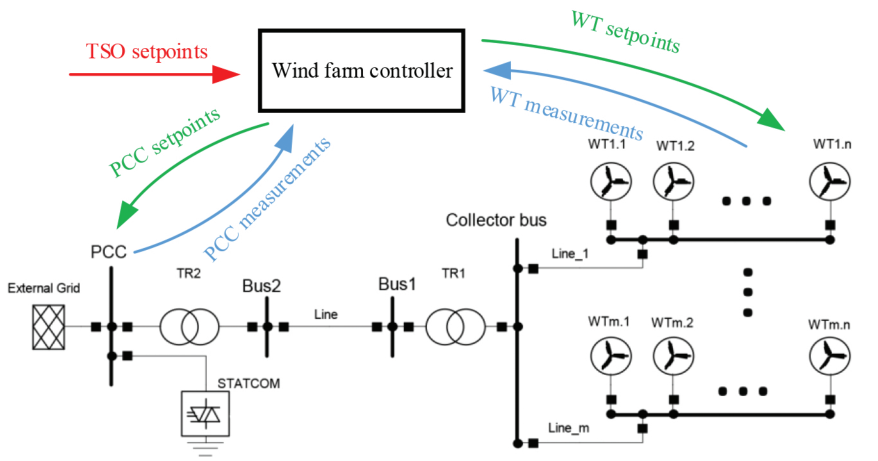

Figure 1.1. Typical wind farm layout.

An overview of the typical control requirements for a wind farm is illustrated in Figure 1.2. During normal operation the wind farm either produces maximum power or is restricted to a set point provided by the wind farm operator. However, there might be situations where it is necessary to activate one of the control functions presented in the diagram to fulfil the grid codes and provide grid support. These control functions have different priorities as noted (e.g. the I. System protection function has the highest priority, followed by II. Protective functions and so on). The active power control is required for cases where the grid frequency (global phenomena) varies from the nominal frequency, while the reactive power is related to voltage fluctuations in the PCC (local phenomena). Based on the measured data in the PCC, such as voltage and frequency, references for the active (P_{PCC}^{ref}) and reactive power (Q_{PCC}^{ref}) are sent to the WFC. The WFC has to ensure that the active and reactive power follow the desired trajectory, by sending P and Q references to the individual wind turbines, based on a dispatch function.

1.2 Problem Statement

This project is carried out in cooperation with Vattenfall, a company which manages both production and distribution of electricity in several European countries.
When a wind farm is acquired, the WFC is typically designed and sold together with the WTs by the same company which produces the WTs. If there is a desire to add WTs from a different manufacturer, they will also be controlled by a different controller. This means that the operators that control the WTs from the Control Center need to have knowledge on how the parameters of each WFC can be adjusted. In order to simplify the procedure of adding new WTs and make the task of the operators easier the company desires to develop their own WFC.
As mentioned previously the company has assets in different countries, so the WFC needs to fulfil all the control functions demanded by the grid codes in each country. In addition

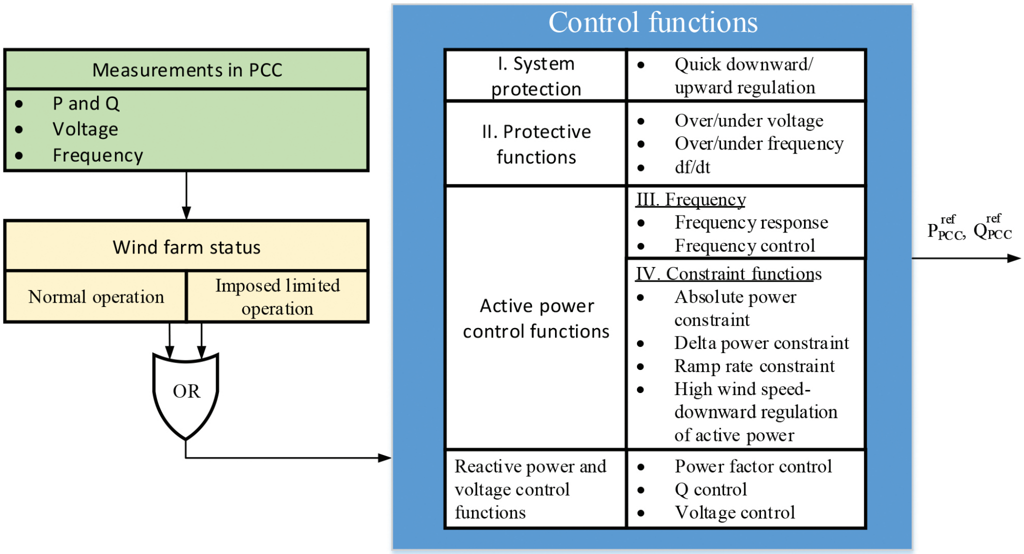

Figure 1.2. Overview of the control requirements for a WFC [5].

to that, the dispatch of power references should be optimized in order to improve system performance.

1.3 Objectives

The objectives that are desired to be achieved during this project are:

1. Develop, implement and tune a wind farm controller, which has the capability to control the active power in the PCC as demanded by the grid operator. In addition to that the WFC must also be able to perform frequency control functionalities to fulfil specific grid codes, i.e. Danish grid codes in this case.
2. Verify robustness of WFC through simulation studies.
3. Implement a suitable dispatch function, which distributes the power references to the individual wind turbines.
4. Validate the developed WFC using Real Time Hardware in the Loop (RT-HIL) approach.

1.4 Limitations

The project at hand deals only with active power control dispatch and frequency related events. In order to simplify the analysis, a series of limitations and assumptions are stated:

- The impact of the harmonics produced by the voltage source converters(VSC) of the wind turbines will not be investigated.
- The control will be performed for normal operating conditions, so it is assumed that the system is balanced.
- A simplified model of the wind turbines will be implemented, i.e. current source model with first order time response.
- An equivalent Thevenin model will be made for the external grid.

- It will not be investigated how the controller behaves during short-circuit events.
- No circuit breakers/surge arresters.
- The active and reactive powers can be controlled individually. This work will only deal with the active power and frequency control.

1.5 Summary

In this chapter the motivation for developing a WFC has been presented. In addition to that the objectives and limitations of the project are underlined. The major goal is to develop a general WFC, which can control active power and frequency, since this would ease the addition of wind turbines from different manufacturers to an existing WF. This would also reduce the number of controllers that the operators in the Control Center operate from approximately 12 to 1.

Wind Farm Controller State of the Art 2

In this chapter an overview of the WFCs available in the scientific literature ,which deal with the dispatch of the active power and frequency control will be presented. Different dispatch strategies are investigated and discussed.

The general scheme of a WFC is depicted in Figure 2.1. The controller can have different objectives such as, maximizing wind farm energy, following a wind farm power reference or minimizing the fatigue load in the farm [6]. In order to achieve these objectives the WFC has access to a number of measurements which describe the state of network (i.e. the available power of each wind turbine, the produced power, voltage and frequency in the PCC, etc.). Based on these measurements and the setpoints provided by the the network operation a dispatch algorithm decides the references of the individual WTs.

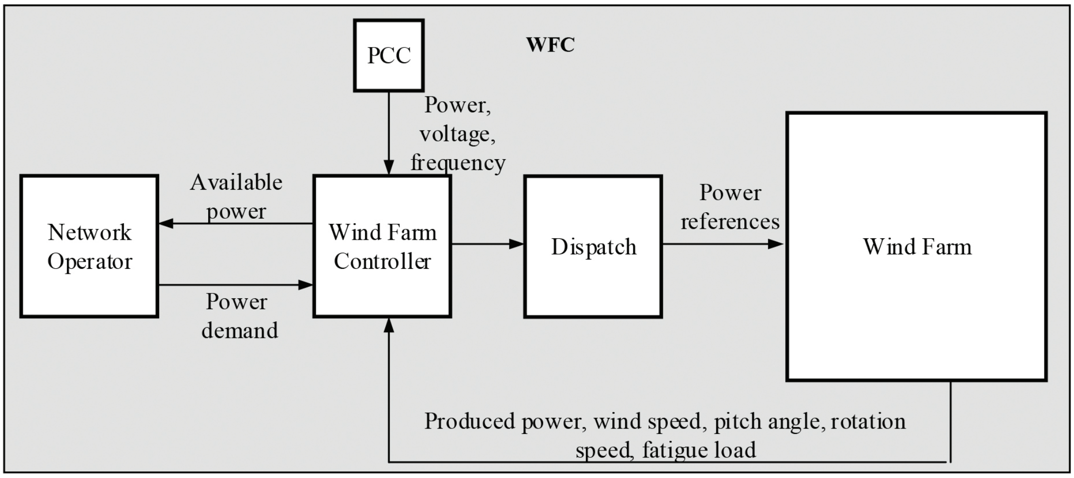

Figure 2.1. General structure of the WFC. [6].

2.1 Wind Farm Controller

The wind farm is a multiple-input multiple-output system, whose order grows with the number of added wind turbines. Furthermore, the system contains numerous non-linearities originating from the power losses in the grid, which depend on the square of the line current and also from the power characteristic of the wind turbines (i.e. available power is a cubic polynomial of wind speed). [7]
Each wind turbine has installed an instrument for measuring the wind speed. An estimation of the available wind power produced by each wind turbine can be obtained

based on the wind speed and a lookup table, which is sent to the WFC. The total available power that the wind turbines can produce is not equal to the total available active power that can be delivered in the PCC due to active power losses in the grid. These losses depend on the grid layout, the external grid voltage and on the active and reactive powers injected in each bus. A method for obtaining the losses as a function of the injected active power is described in [8], using the following quadratic expression:

$$P_L = \sum_{i=1}^{n}\sum_{j=1}^{n} P_i B_{ij} P_j + \sum_{i=1}^{n} B_{0i} P_i + B_{00} \tag{2.1}$$

where P_L are the total power losses in the system, B_{ij}, B_{0i} and B_{00} are loss coefficients. These coefficients are obtained for a specific operating point based on a load flow. Reasonable accuracy can be obtained for operating points close to the point where the loss coefficients were calculated. To simplify the calculations even more the linear and constant term from (2.1) can be omitted.
The main objective of the WFC is to ensure that the wind power plant delivers the requested P and Q in the PCC. Furthermore, it must also provide an estimation of the losses, to obtain an approximate value of the deliverable power in the PCC, to ensure that the reference provided by the operator can be tracked.
The diagram of a typical main controller of the wind farm is presented in Figure 2.2.

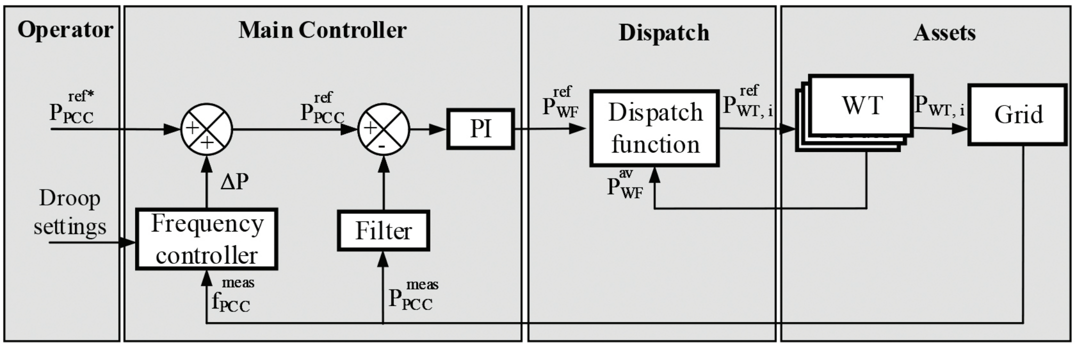

Figure 2.2. Detailed block diagram of the main controller.

The WF operator or TSO sends a set-point for the desired power production, P_{PCC}^{ref*}. In this diagram, the reactive power set point is omitted since it is desired to achieve a unity power factor, which can be achieved either by providing reactive power from the grid side converter of the WTs or by a STATCOM. For frequencies in the dead-band specified by the grid codes, $P_{PCC}^{ref*}=P_{PCC}^{ref}$. If the frequency response or frequency control functions are active the set point in the PCC is adjusted according to the droop specifications $P_{PCC}^{ref}=P_{PCC}^{ref*}+\Delta P$. The actual active power, P_{PCC}^{meas} is measured in the PCC and filtered to reduce the amplitude of the noise and achieve an average value. The error between the reference and measured values is run through a PI controller with anti wind-up and generates a corrected value P_{WF}^{ref}, which compensates for the power losses present in the grid [9].
The anti wind-up of the integrator is necessary for the case when the demanded power is higher than the available power. Without anti wind-up the output of the integrator would continue to rise as long as there is a tracking error. In [10] a design method for resetting

the integrator is presented. The reset is made based on the pitch angles of the WTs. In the proposed method the integrator gain is adjusted based on a lookup table, but there are not given any details on how this is made.
Additional controllers have been mentioned in the literature such as proportional, fuzzy logic controllers, model predictive controllers, etc. [11], but there is no evidence that these control strategies have been implemented in real applications. On the other side, the PI-controller has been implemented in the Danish WF at Horns Rev.
The dispatch function block sends power references to the individual turbines based on different optimization algorithms. An overview of possible dispatch methods is presented in the next section.

2.2 Dispatch Strategy

Various methods for dispatching the active power can be encountered in the available scientific literature. The most simple method is to equally dispatch the active power between the individual WTs, but this is not desired since it does not take into account the spacial variation of wind speeds, the structural stress on the wind turbines and the losses present in the system. A more convenient approach, which has been mentioned in [12] [13] is to send the WT references proportional to the total available power to avoid overloading of some WT as given by:

$$P_{\mathrm{WT,i}}^{\mathrm{ref}} = \frac{P_{\mathrm{WT,i}}^{\mathrm{av}}}{P_{\mathrm{WF}}^{\mathrm{av}}} \cdot P_{\mathrm{WF}}^{\mathrm{ref}} \tag{2.2}$$

where the superscript 'av' denotes the available power. The total available power is given by:

$$P_{\mathrm{WF}}^{\mathrm{av}} = \sum_{i=1}^{n} P_{\mathrm{WT,i}}^{\mathrm{av}} \tag{2.3}$$

Additional methods have been proposed to optimize different parameters. In [4] a predictive-adaptive control is proposed, which can satisfy one of the two major goals (1.Accurately track the power reference or 2.Provide smooth power output) based on algorithms which make use of long term weather forecast (predictive) and short-term weather forecast (adaptive). In [12] a method to optimize the tower torque using a weighted cost function is presented. A method which is intended to minimize the active power losses in the grid is presented in [14]. However, there are no mentions of such optimization methods that are implemented on real WFs. Most of the simulations are done with WFs that consist of a small number of WTs (up to 10). This is because the optimization process is typically a complex algorithm which depends on many variables which can change in time (e.g. wind speed, external grid voltage, etc.).

2.3 Summary

The state of the art of WFC has been presented in this chapter. Even though, numerous optimization strategies have been presented in the scientific literature, it seems that the only concept that has been proven in an actual WF is based on a main regulator with a PI-controller. This is therefore also the structure that is chosen for this project.

System Characterization and Network Modelling 3

The major components of an actual offshore wind farm are presented in this chapter followed by a description of how these components (i.e. external grid, wind turbines and cables) are modelled. This will form the test platform for the controllers which will be developed in the following chapters.

The performance and robustness of the controllers which will be developed during this project will be assessed using the model of an actual wind farm, i.e. Horns Rev 1, which is situated on the West coast of Denamrk. The wind farm is rated at 160 MW and consists of 80 WTs, each turbine being able to deliver 2 MW. The WTs are installed on 10 feeders, each feeder containing 8 WTs. The electrical diagram of the WF can be seen in Figure 3.1 and consists of 83 buses.

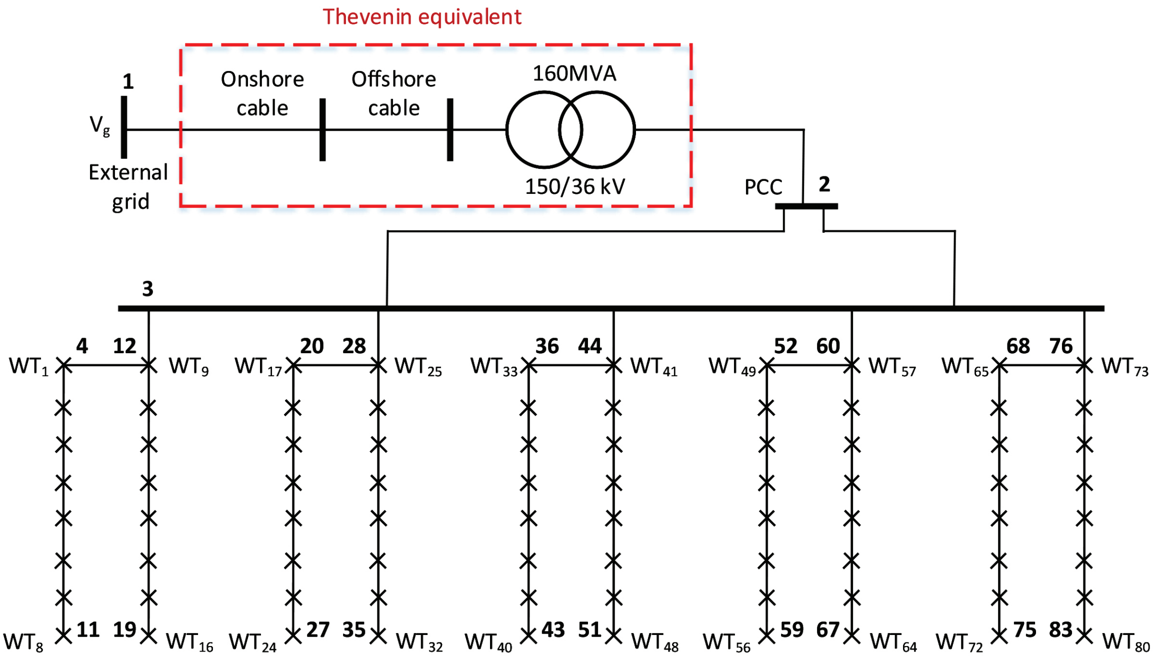

Figure 3.1. Single line diagram of the WF.

The grid components that connect the External grid with the PCC are managed by the TSO. The parameters of these components are unknown. This part of the grid will therefore be represented with its Thevenin equivalent.

3.1 Modelling of the Lines

The theoretical representation of the overhead lines or underground cables can be done with a π model, which is presented in Figure 3.2. This lumped parameter approach is suitable for dynamic stability studies and load flows of power systems [8]. The lines are represented by their series resistance R, reactance X and half of the total shunt admittance Y connected at each end of the line.

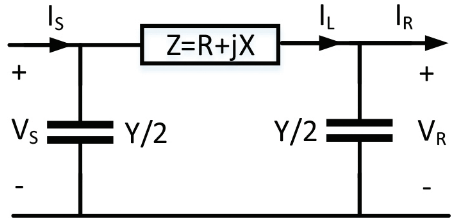

Figure 3.2. Nominal π model of the line.

The values are known for a specific layout and usually provided in per unit length. The shunt admittance is expressed as:

$$Y = j\omega C \tag{3.1}$$

3.2 Modelling of the Wind Turbines

Modern offshore wind farms contain a large number of WTs, e.g. the London Array wind farm in the UK consists of 175 individual WTs. In order to simulate the behaviour of the grid containing the WTs it is necessary to develop a model, which is simple enough to allow simulation of the system in a reasonable amount of time. On the other side it should also be able to capture the main dynamics of the WTs. A model which can capture the fast variations in wind speeds, the dynamics of the converters and other components such as filters is not suitable, since it would necessitate very small simulation time steps. A simplified approach is therefore necessary, where the WT is modelled based on performance of power output characteristic as shown in Figure 3.3, which has as inputs the wind speed (v) and power references and as outputs the available active power and the generated powers. The control systems of the wind turbines are able to track the provided set-points (the static error is in general close to zero), so the WT can be treated as a PQ generation source [6].

The model of the WT proposed in [15] and shown in Figure 3.4 is used in this project. The same model has also been proposed in [4], with an additional term that simulates the effect of very fast wind transients on the active power output. The rotor inertia has a smoothing effect on the time and spacial variation of the wind. This is taken into consideration by applying a first order filter, with the time constant τ. According to [16], τ is defined as:

$$\tau = \tau_0 \frac{v_{rated}}{v_{meas}} \tag{3.2}$$

where τ_0 is the natural time constant (defined as the time it takes to reach rated speed from standstill) and v_{rated} is the rated wind speed of the WT. The value of τ_0, depends on the rated power of the WT as it can be observed in Figure 3.5.

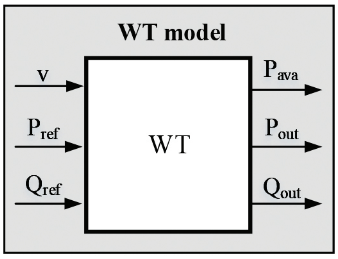

Figure 3.3. Simplified diagram of a WT.

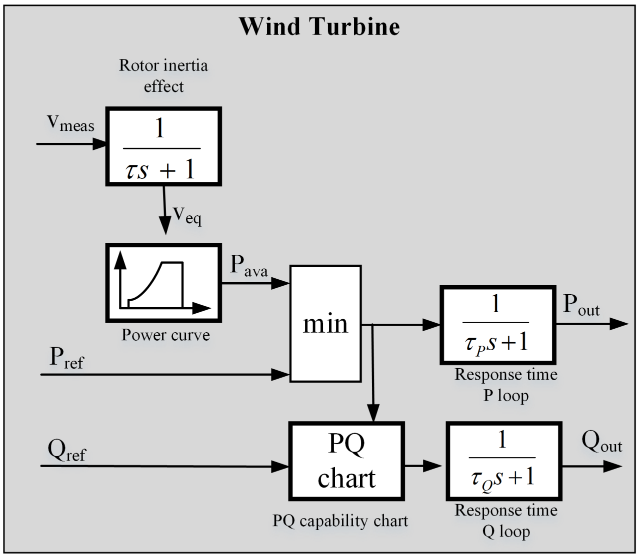

Figure 3.4. Detailed diagram of the proposed WT model.

The maximum available power that the wind turbine can produce can be derived from the measured average wind speed, v_{meas} based on a known power curve of the WT. For wind speeds below 3-4 m/s the wind turbine does not produce any power. Between this point and the rated speed, the available power depends on the wind speed with a cubic function. The rotor speed tracks an optimized curve and the pitch angle is kept to zero to maximize the power output. Above the rated speed the WT produces the rated power by adjusting the pitch angle. For wind speeds higher than 25 m/s the wind turbine is shut down.

For WTs in the MW class, there are two main technology types, which are both based

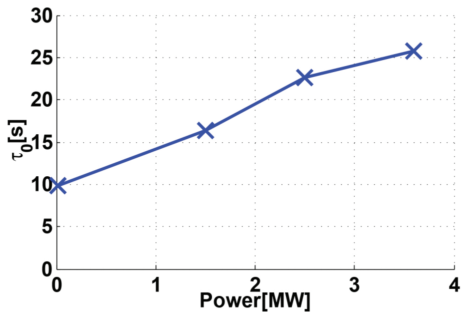

Figure 3.5. Natural time-constant of commercially available wind turbines [16].

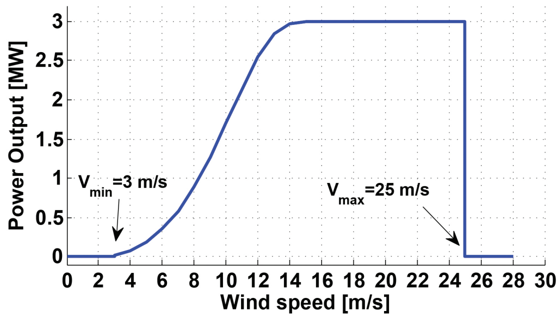

Figure 3.6. Power curve of the Vestas V112 WT. [17]

on variable speed operation: type III-Doubly Fed Induction Generator(DFIG) and type IV-full scale converter (FSC) [18]. For DFIG based WTs the capability to deliver reactive power depends on the delivered active power. For type IV based WTs, where the converter transfers all the power, the amount of the reactive power that can be delivered by the converters is fixed. However, there is also a dependence on the active power, caused by the power losses in the transformer that connects the WT to the Point of Connection (PoC). This effect is taken into account by the 'PQ chart' block. The P and Q loops are treated as first order systems with the response times τ_p and τ_Q. For the P loop loop a typical response time has the value τ_P= 1 s. For the Q loop the response time is approximately

100 ms [17]. According to the data sheets, P_{ref} can not change faster than 0.1 p.u./s, due to technical limitations .

3.3 Modelling of the External Grid

As mentioned previously the parameters of the external grid are unknown, but they are typically provided by the TSO within a specific range. A common approach to model the grid is to replace the actual grid with its Thevenin equivalent, consisting by a voltage source (with magnitude V_g) behind grid impedance (Z_g) [19].

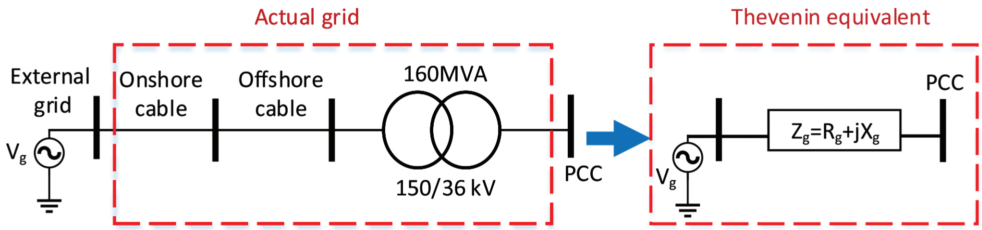

Figure 3.7. Thevenin equivalent of the external grid.

The magnitude of R_g and X_g is calculated from the short-circuit ratio (SCR) of the grid and the X_g/R_g ratio (XR). The SCR is defined as the ratio between short-circuit power (S_k) and nominal power in the PCC (P_{WF}^{rated}):

$$SCR = \frac{S_k}{P_{WF}^{rated}} \tag{3.3}$$

The magnitudes of the grid resistance and reactance are given by:

$$Z_g = \frac{V_g^2}{S_k} \tag{3.4}$$

$$X_g = \frac{Z_g \cdot XR}{\sqrt(1 + XR^2)} \tag{3.5}$$

$$R_g = \frac{X_g}{XR} \tag{3.6}$$

If the SCR is high, it means that the grid impedance is low. This indicates a stiff grid, which means that the voltage drop between the external grid and the PCC is small. According to [3] a grid is stiff for SCR>20. A typical value for X/R is around 10.

3.4 Summary

This chapter contains a description on how the different grid components are modelled. The cables are treated as lumped π sections. The external grid is modelled in terms of the SCR and XR. The WTs are modelled as current source.

Model Verification and Plant Characterization 4

This chapter contains a comparison between the Simulink model, which is developed based on the equations presented in Chapter 3 and a power systems tool. In addition to that, a series of simulations is performed to determine the impact of different parameters on the losses. Based on the knowledge gained here, a simplified version of the plant transfer function is obtained.

A model of the WF has been implemented in Matlab Simulink. In order to asses if the steady-state operation of the model is correct, a series of simulations will be performed and the results will be compared with the results of a load flow program based on a Newton-Raphson solver. The assessment will be made based on the bus voltages and line losses.
The load flow calculates the magnitudes and angles of the bus voltage phasors. The network can be described by the following system of equations:

$$[I] = [Y] \cdot [V] \tag{4.1}$$

where I is a vector containing the injected currents in the buses, V is the bus voltage and Y is the admittance matrix [8]. The injected currents can be calculated as:

$$I_i = \frac{P_i - jQ_i}{V_i^*} \tag{4.2}$$

When the line currents and all the bus voltages are known, the losses can be calculated easily.
An approximation for the voltage drop across the line, which has been derived in [20] is given by:

$$\Delta V = \frac{1}{V_g}(R_g P_{PCC} + X_g Q_{PCC}) \tag{4.3}$$

4.1 Model Verification

4.1.1 Comparison of Simulink Model with Load Flow

The steady-state behaviour of the Simulink model is verified against a commercial power system toolbox developed by [8] and implemented in Matlab. The assessment criteria is based on the bus voltage magnitude and the losses in the WF. This is done for different loadings (i.e. 0.2 and 1 p.u.) and different voltage magnitudes of the external grid (i.e. 0.9, 1 and 1.13 p.u.). The SCR and the XR ratio of the grid impedance of the external grid are set to 10. The results of both the simulations and the load flows can be seen in Figure 4.1 and Figure 4.2 respectively.

Similar behaviours can be observed with small differences in the bus voltage magnitudes

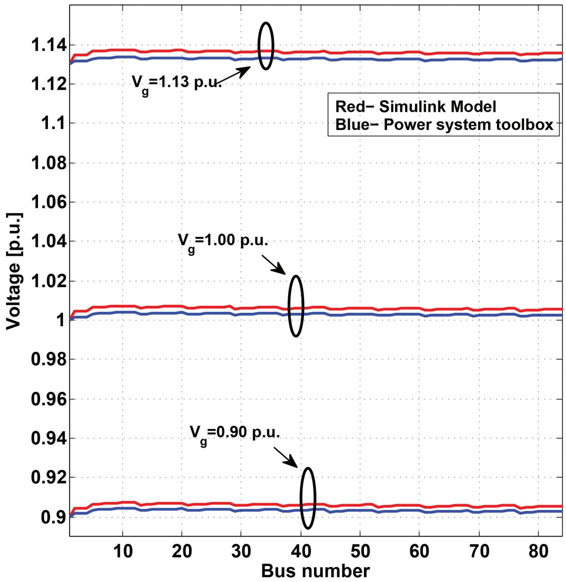

Figure 4.1. Magnitude of the bus voltages at P_{WF}^{out}=0.2 p.u. and different V_g.

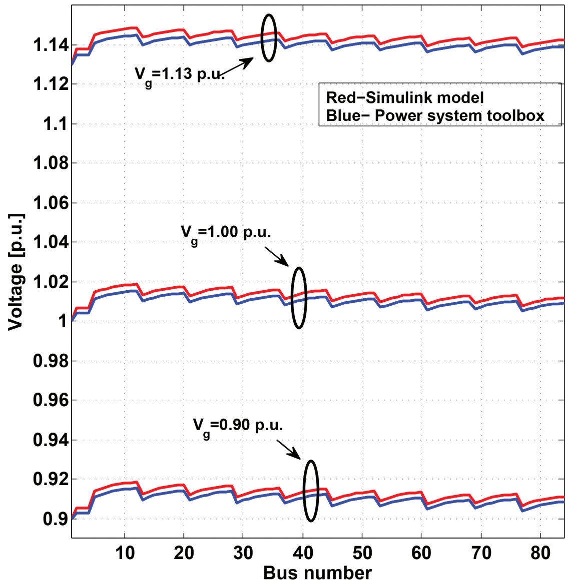

Figure 4.2. Magnitude of the bus voltages at P_{WF}^{out}=1 p.u. and different V_g.

and the total losses. The absolute values of the errors are summarized in Table 4.1.1.

P_{WF}^{out}[p.u.]	V_g	$V - error$[%]	$P_{WF}^{loss} - error$[%]
0.20	0.90	0.3	0.28
	1.00	0.3	0.75
	1.13	0.3	1.61
1.00	0.90	0.3	0.83
	1.00	0.3	0.56
	1.13	0.3	0.52

Table 4.1. Comparison between load flow results and Simulink model for various operating points.

The maximum deviation of the voltage magnitude is 0.3 % for all the investigated operating points. The maximum deviation of the losses is 1.61 %. The magnitude of the differences is acceptable, so the model developed in Simulink is suitable for the assessment of the steady-state behaviour.

4.2 Characterization of the WPP Transfer function

The methodology used to derive the plant transfer function is presented in this section. The impact of the various electrical parameters, such as the voltage of the external grid,V_g the short circuit ratio of the grid, SCR, XR ratio of the grid and the injected reactive power is investigated. This is done in order to obtain an estimation of the total losses (P_{WF}^{loss}) in the wind farm network and to obtain a more accurate estimation of the active power that can be delivered in the PCC. The power delivered in the PCC can be calculated by:

$$P_{PCC}^{out} = P_{WF}^{out} - P_{WF}^{loss} \tag{4.4}$$

where P_{PCC}^{out} is the power measured in the PCC, P_{WF}^{out} is the total power generated by the wind turbines and P_{WF}^{loss} are the losses in the grid. The losses can be expressed as the following function:

$$P_{WF}^{loss} = f(V_g, P_{WF}^{out}, Q_{WF}^{out}, SCR, XR) \tag{4.5}$$

The diagram of the plant is presented in Figure 4.3. Due to a large number of buses and the complexity of the system an analytical expression for the losses is a not a viable solution. In addition to this, different wind speeds lead to different operation points of WTs hence different losses/loading. Therefore, some simplifications are needed in order to obtain a transfer function, which is suitable for classical SISO control theory. The plant is therefore described by a first order transfer function with the response time equal to the response time of the WTs and a gain, K_{loss}, which depends on V_g, SCR, etc. This can be done by assuming that the WTs provide the same output power.

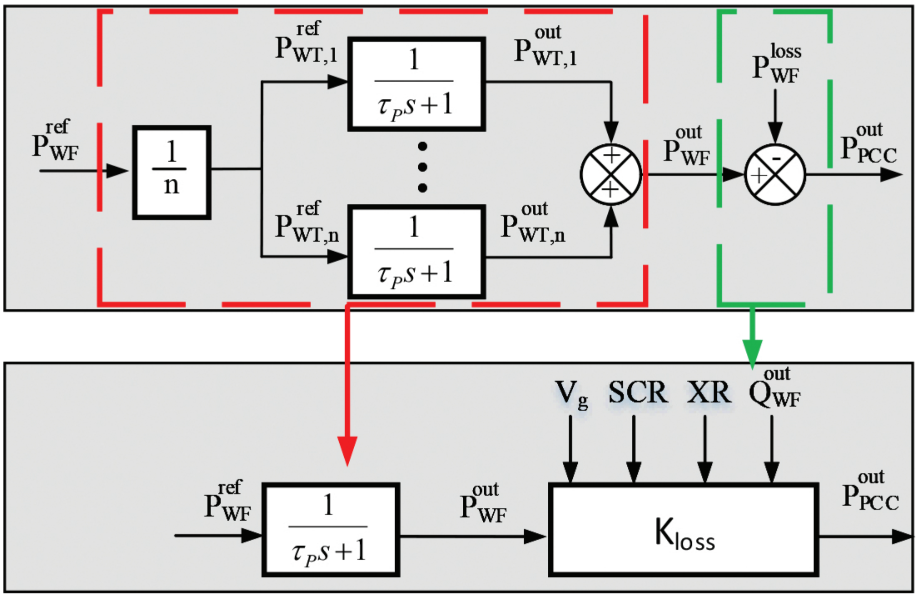

Figure 4.3. Diagram of the active power transfer function.

In the following sections an attempt will therefore be made to obtain a function for the losses and determine which parameters have the greatest impact on the losses. This is done by performing load flows with the parameters of the wind farm described in Chapter 3.
The external grid voltage is rated at 150kV and according to [5], V_g can vary between 0.9 and 1.13 p.u. at this voltage level. A typical value for the SCR and XR is 10, which will be considered as the base case. These parameters might vary, so the following cases will be simulated to obtain a mapping of the losses for various operating conditions:

- Test case 1. Q_{WF}^{out}=0; SCR=10; XR=10; P_{WF}^{out} is varied between [0;1] p.u. for each V_g=[0.9; 0.95; 1 ; 1.05; 1.13] p.u.

- Test case 2. Q_{WF}^{out}=0; XR=10 ;P_{WF}^{out} is varied between [0;1] p.u. for each V_g=[0.9; 0.95; 1 ; 1.05; 1.13] p.u. and SCR=[5; 10; 25].
- Test case 3. Q_{WF}^{out}=0; SCR=10 ;P_{WF}^{out} is varied between [0;1] p.u. for each V_g=[0.9; 0.95; 1 ; 1.05; 1.13] p.u. and XR=[5; 10; 20].
- Test case 4. SCR=10; XR=10 ;P_{WF}^{out} is varied between [0;1] p.u. for each V_g=[0.9; 0.95; 1 ; 1.05; 1.13] p.u. and pf=[0.98_{cap}; 0.96_{ind}].

4.2.1 Case 1- Influence of Grid Voltage and WF Output Power

For this case it is desired to obtain the losses as a function of the WF output power and the external grid voltage, for constant SCR and XR values and 0 reactive power. The losses can therefore be expressed as:

$$P_{WF}^{loss} = f(V_g, P_{WF}^{out}) \tag{4.6}$$

The results of the load flows performed for this scenario can be seen in Figure 4.4. The highest losses are obtained for V_g=0.9 p.u. as expected, since the line currents at this point have the highest magnitude. At full loading (i.e. P_{WF}^{out}=1), the losses increase from 0.005 p.u. to 0.008 p.u. for V_g=1.13 and V_g=0.9 respectively. This indicates that V_g has a significant impact on the losses. Furthermore, the total losses have a square dependency on the loading.

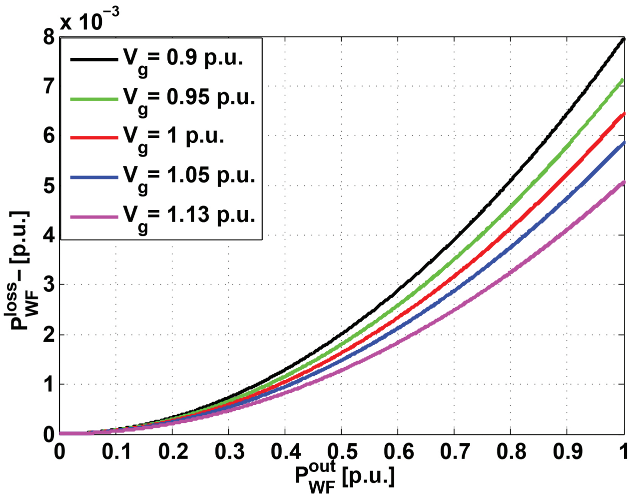

Figure 4.4. Active power losses in the WF network at SCR=10, XR=10 and pf=1 for different V_g and output power.

The 'Curve Fitting Toolbox' from Matlab has been used to obtain the expression of the function described in Eq. 4.6. The fitting was done with both 2^{nd} and 3^{rd} order polynomials, which can be seen in Figure 4.5 and Figure 4.6.

The fitted curves are described by the following equations:

- Second order:
  $P_{WF}^{loss}(V_g, P_{WF}^{out}) = p_{00} + p_{10}V_g + p_{01}P_{WF}^{out} + p_{20}V_g^2 + p_{11}V_gP_{WF}^{out} + p_{02}(P_{WF}^{out})^2$
- Third order:
  $P_{WF}^{loss}(V_g, P_{WF}^{out}) = p_{00} + p_{10}V_g + p_{01}P_{WF}^{out} + p_{20}V_g^2 + p_{11}V_gP_{WF}^{out} + p_{02}(P_{WF}^{out})^2 + p_{21}V_g^2P_{WF}^{out} + p_{12}V_g(P_{WF}^{out})^2 + p_{03}(P_{WF}^{out})^3$

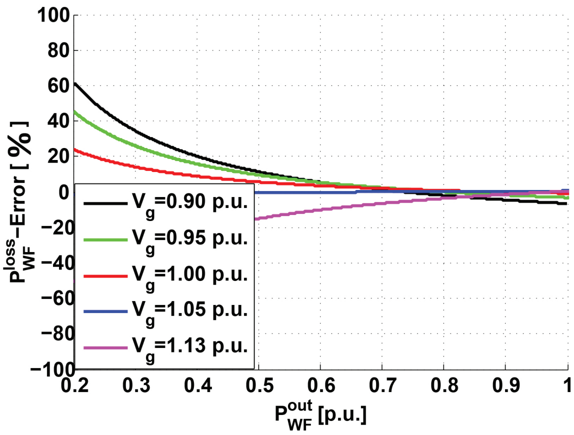

Figure 4.5. Error between second order polynomial fit and simulation.

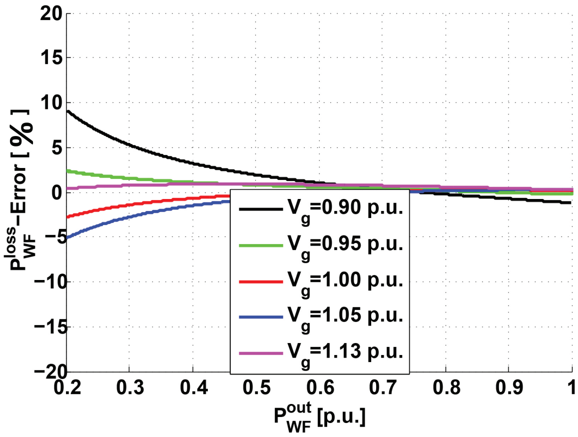

Figure 4.6. Error between third order polynomial fit and simulation.

The parameters of the equations are presented in Table 4.2.1.

Coefficient	2^{nd} order pol.	3^{rd} order pol.
p_{00}	0.0009525	-0.0003032
p_{10}	-0.002112	0.0005865
p_{01}	0.01092	0.01618
p_{20}	0.001151	-0.0002779
p_{11}	-0.01041	-0.031
p_{02}	0.005901	0.01776
p_{21}	-	0.01475
p_{12}	-	-0.01105
p_{03}	-	-0.0001819

Table 4.2. Coefficients of fitted polynomial.

For the second order polynomial the expression is very inaccurate especially for low loadings. The 3^{rd} order approximation is a much better fit, i.e. the error is below 5% for loading above 0.3 p.u.. For this reason the 3^{rd} order polynomial will be used to calculate the losses.

4.2.2 Case 2- Influence of SCR

In this series of simulations it is desired to determine how the SCR affects the losses. In order to do this, load flows have been performed with SCR∈[5; 10; 25] at different voltages and varying output power. The results are illustrated in Figure 4.7 and Figure 4.8.

For SCR=5 the deviation is between [-4;2]%. For SCR=25 the error is less than 1%. The behaviour is as expected, i.e. for higher SCR, which represents a stiff grid, the error is low since the voltage drop across the line is also low. Even though there is some error in the active power losses for different SCR values, it can be said, that within this range the SCR does not have a significant impact on the losses.

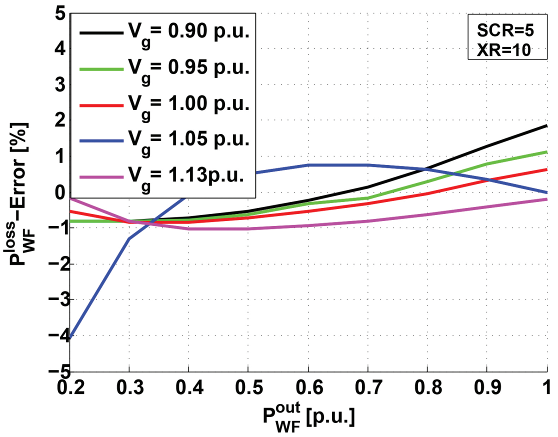

Figure 4.7. Losses error for SCR=5 compared with SCR=10.

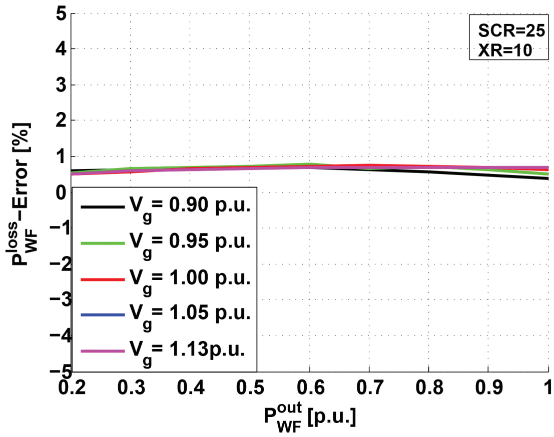

Figure 4.8. Losses error for SCR=25 compared with SCR=10.

4.2.3 Case 3- Influence of XR

The results of load flows performed with different XR ratios can be seen in Figure 4.9 and 4.10. The losses are lowest for XR=5, since the voltage drop across the grid impedance is highest in this case, which means that the voltage in PCC is highest. This can be explained with help of Eq. 4.3, which indicates that the voltage drop depends mainly on the active power, since the power factor in the PCC will be close to 1. The SCR is set to 10, which means that when XR decreases, R increases and the voltage drop also increases, so the voltage in the PCC becomes higher, leading to lower losses (negative error).

When the XR changes, the largest deviation occurs at full load and for V_g=0.9 p.u.

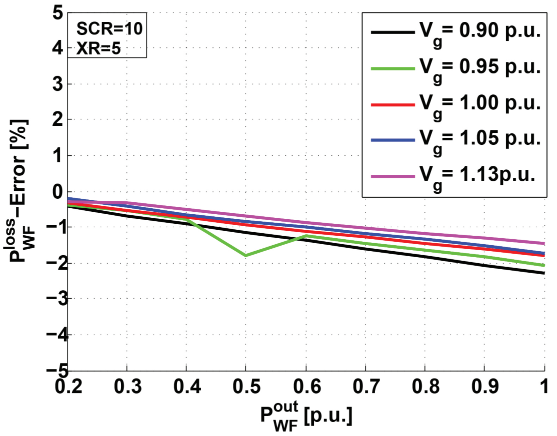

Figure 4.9. Losses error for XR=5 compared with XR=10.

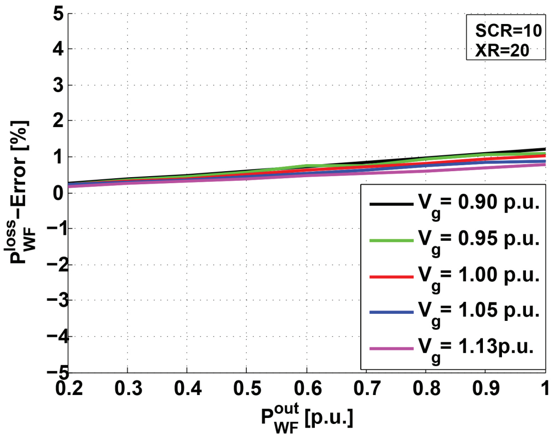

Figure 4.10. Losses error for XR=20 compared with XR=10.

From XR=10 to XR=5 the change is maximum -2.3% and from SCR=10 to SCR=20 the deviation is maximum 1.2%. The XR ratio is typically known for a specific grid, but based on the results it is shown that even though the values might change around the initial value due to tap-changers for example, the absolute magnitude of the deviation of the losses is within some acceptable boundaries, i.e. maximum 2.3 % for the worst case.

4.2.4 Case 4-Influence of Reactive Power Injection

In this case, the impact of reactive power generation from the WTs is investigated. Two limits have been chosen (0.96_{ind} and 0.98_{cap}), which are typical for a DFIG in the MW range. The results of the simulations can be seen in Figure 4.11 and Figure 4.12 respectively.

It can be mentioned that the reactive power has a significant impact on the losses, e.g.

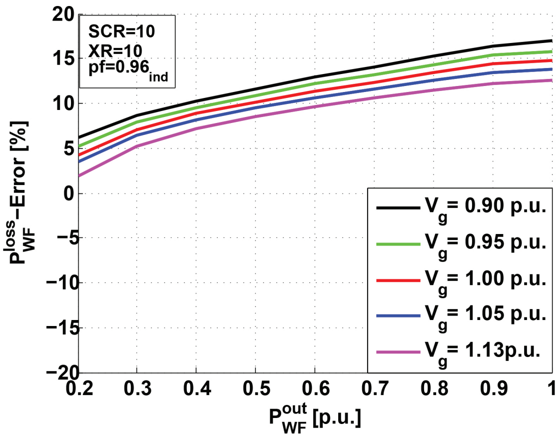

Figure 4.11. Losses error for pf=0.96_{ind} compared with pf=1.

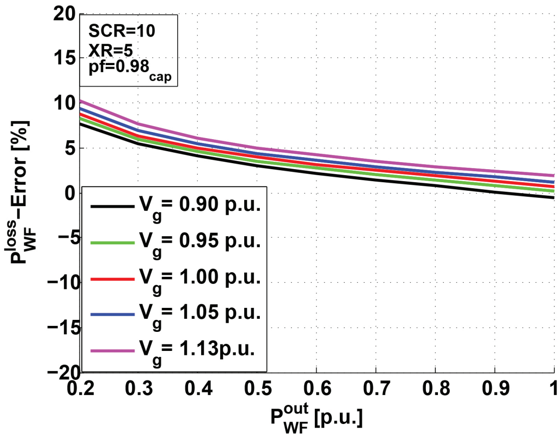

Figure 4.12. Losses error for pf=0.98_{cap} compared with pf=1.

the error between pf=1 p.u. and pf=0.96_{ind} can be as high as 17%, depending on the voltage of the external grid. However, during normal operation the power factor is set to unity.

4.3 Summary

In this chapter a verification of the steady-state model has been made, by comparing it with traditional power systems tools. The deviation between the developed Simulink model and the toolbox is 0.3 % in the bus voltages and 1.6 % in the active power losses. These values are acceptable, therefore the model is used to investigate the influence of different parameters, such as SCR, XR, external grid voltage, loading and power factor on the active power losses in the WF grid. A simplified model of the plant is also obtained, which is needed for the design of the controller.

Controller Requirements, Design and Tuning 5

This chapter contains a review of the Danish grid codes which deal with active power and frequency control. The methodology used to design and tune the controllers is also described here. Finally, the controller is verified for different operating conditions.

5.1 Overview of the Grid Codes Related to Active Power and Frequency Control

In this section, an overview of the grid codes related to active power and frequency control is presented.

5.1.1 Danish Grid Codes

According to [5], there are four types of WPP, characterized by their nominal power and the magnitude of the voltage in the PCC. These four types are:

- A2. Plants above 11 kW up to and including 50 kW.
- B. Plants above 50 kW up to and including 1.5 MW.
- C. Plants above 1.5 MW up to and including 25 MW.
- D. Plants above 25 MW or connected to over 100 kV.

The WF analysed in this work is rated at 160 MW, so only the requirements regarding type D plants will be presented. The requirements are related to active power control, frequency control and system protection control.

5.1.1.1 Active Power Constraint Functions

All the active power control in the PCC needs to be done within an accuracy of 2% of the nominal power,P_n of the WPP.

a. Absolute Power Constraint

This function can be activated to limit the amount of active power in the PCC, based on a setpoint received from the TSO. The control action should be commenced in 2 seconds and be completed in 10 seconds.

b. Delta Power Constraint (Spinning Reserve)

The Delta power constraint is activated to limit the generated power in proportion to the available active power. This constraint function is useful for cases where upward regulation is needed in order to provide frequency control. The control action should be commenced in 2 seconds and be completed in 10 seconds.

c. Ramp Rate Constraint

The ramp rate constraint is used to limit fast changes in the active power. This is done in order to contribute to the stability of the system, since fast changes in the active power might lead to undesired behaviour. The maximum value of the ramp rate is 100 kW/s. The control action with a new ramp rate should be commenced in 2 seconds and be completed in 10 seconds.

An overview of the active power constraint functions can be seen in Figure 5.1.

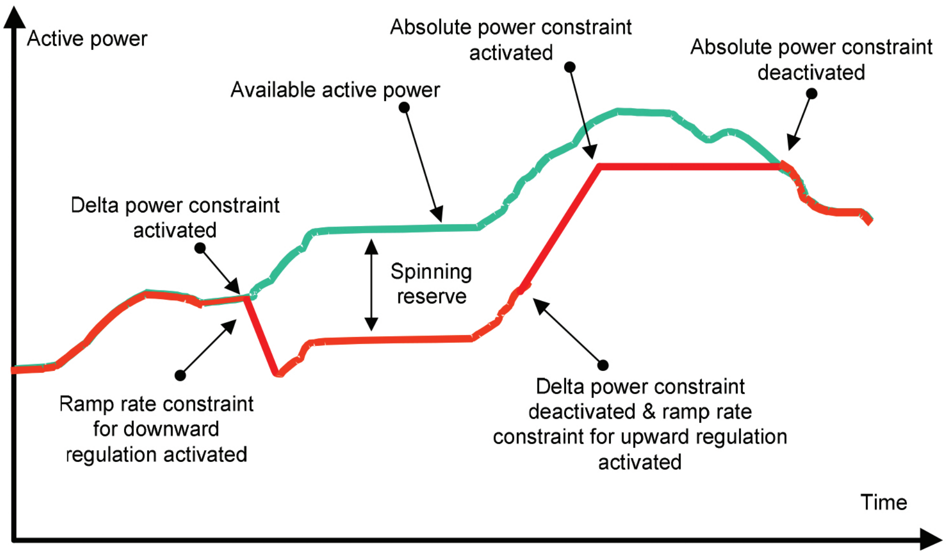

Figure 5.1. Graphical illustration of the active power constraint functions. [5]

5.1.1.2 Frequency Control Functions

For cases where the grid frequency deviates from the nominal frequency (50 Hz), the WPP should provide frequency support by changing its active power output based on a predetermined function. Two types of control can be distinguished: frequency response and frequency control.

a. Frequency Response

The frequency response requirements are illustrated in Figure 5.2. If the grid frequency exceeds f_R, the WPP should change its output based on the droop specified by the TSO. Droop is defined as the change in active power as a function of grid frequency. The value of the droop is between 2-12 % of P_n. The standard value for the droop is 4 %. The standard value for f_R is 50.2 Hz. If f_R is set to 52 Hz the function is not activated. The control must be commenced in 2 seconds and completed in 15 s.

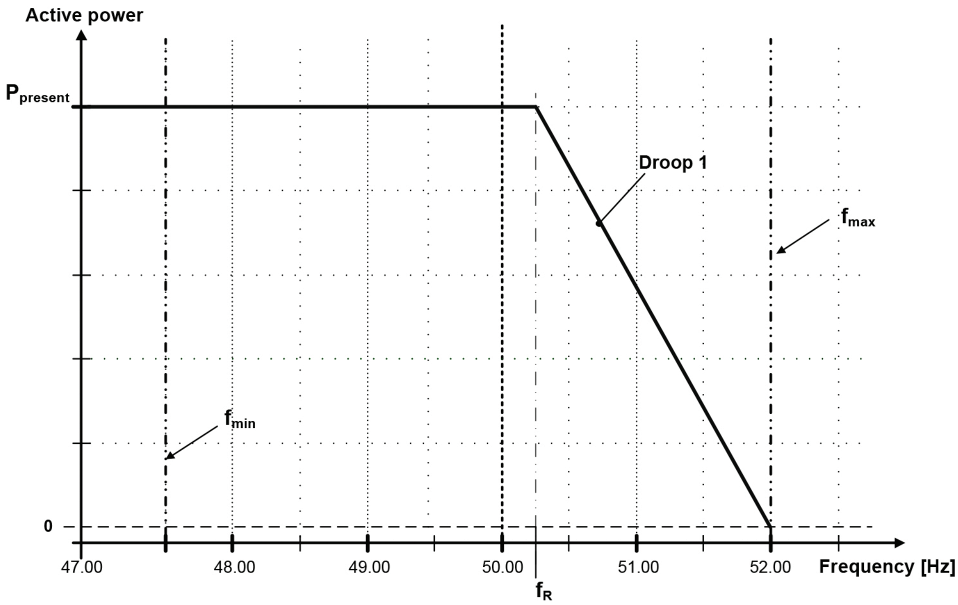

Figure 5.2. Graphical illustration of the frequency response function. [5]

b. Frequency Control

Frequency control is used to limit the active power output for frequencies above f_1 as illustrated in Figure 5.3. Different values for the droop can be specified, depending on the interval where the grid frequency lies. The control should be initiated no later than 2 seconds and be completed in 15 seconds. If the upward regulation exceeds 10 % of P_n the response time may be increased. For regulation events above f_5, the active power may be increased only when the frequency has dropped below f_7.

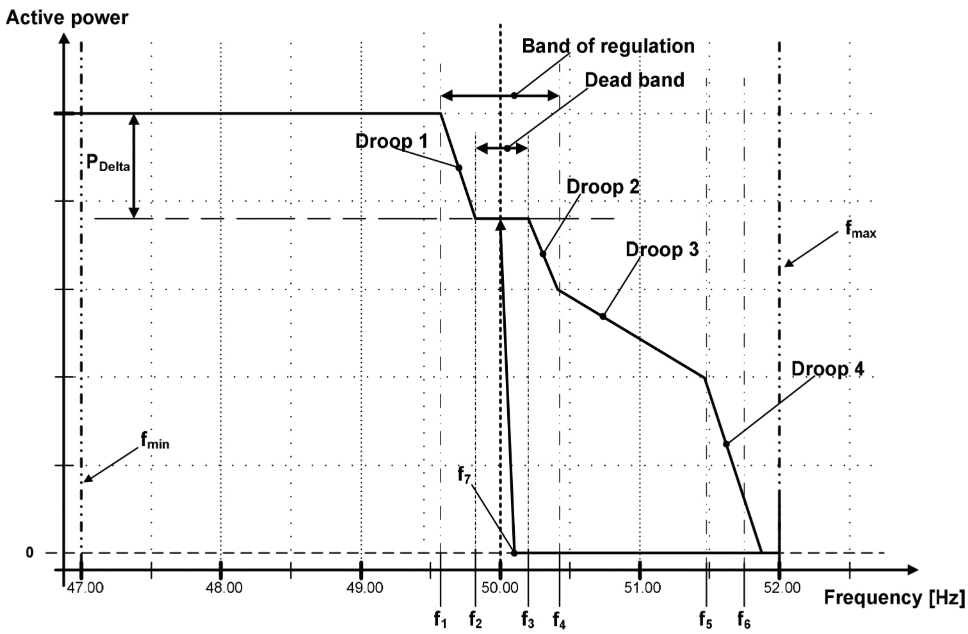

Figure 5.3. Graphical illustration of the frequency control function. [5]

5.1.1.3 System Protection

The WPP must have at least five configurable step options to quickly regulate the active power upward or downward as desired by the TSO. The recommended values for the steps are: [0 25 40 50 70]% of P_n. Control must be commenced in 1 second and be completed in 10 seconds. For upward regulation the response time may be higher.

5.2 Performance Assessment Criteria and Tools

According to the grid codes, the settling time should be 10 s for a power reference change of 0.1 p.u. of P_n. This value might however increase if the change is higher. The steady state error should be below 2 % of P_n. The controller will therefore be designed and assessed based on these requirements. In addition to this, the closed loop control system should be stable and have no overshoot.
Stability- For systems developed in the continuous time domain, the stability criterion requires that all the poles of the closed transfer function must be placed in the left half of the complex time domain. For discrete systems, the modulus of the poles should be less than 1.
Bandwidth-The bandwidth is defined as the frequency, where the gain of the closed loop system drops by 3dB.
Gain margin and phase margin- The phase margin is defined as the difference between the phase of the response and -180° when the gain is 0 dB. The gain margin is defined as the inverse of the gain where the system becomes unstable (i.e. when the phase is -180°). Typical values for the phase margin are 30-60°. These values combined with a gain margin of 3 yields a stable system with a reasonable response time.
Root locus- This is a tool which can be used to obtain the placement of the closed loop poles as a function of the controller gain. [21]
The controller requirements are the following:

- Steady-state error: $<$ 2% of P_n
- Settling time to a step of 0.1 p.u.: $<$10 s
- No overshoot
- Stable system

5.3 Controller Design and Tuning

The diagram of the controlled system is presented in Figure 5.4. The error between the reference and the measured values in the PCC serves as the input to the controller. The controller generates an appropriate reference for the WF power production.

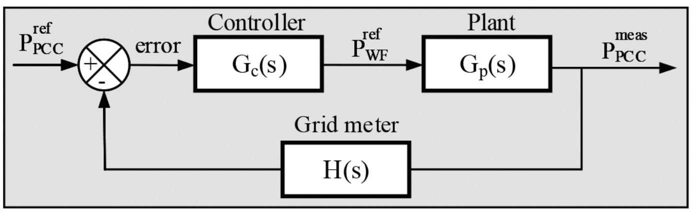

Figure 5.4. Closed loop control scheme

The closed loop transfer function [21] can be expressed based on block diagram calculations:

$$G_{cl}(s) = \frac{P_{PCC}^{meas}(s)}{P_{PCC}^{ref}(s)} = \frac{G_p(s)G_c(s)}{1 + G_p(s)G_c(s)H(s)} \tag{5.1}$$

The transfer function of the plant has been obtained previously and it can be described as:

$$G_p(s) = \frac{P_{PCC}^{meas}(s)}{P_{WF}^{ref}(s)} = \frac{K_{loss}}{\tau_P s + 1} \tag{5.2}$$

The loss coefficient, K_{loss} can be expressed as:

$$K_{loss} = \frac{P_{WF}^{out} - P_{WF}^{loss}}{P_{WF}^{out}} \tag{5.3}$$

K_{loss} does not have a fixed value and it can be expressed as a cubic function of the total output power and the grid voltage as shown in Section 4.2. The controller will therefore be designed for the specific operating point presented in Figure 5.5. The parameters of this operating point are: SCR=10, XR=10, Q_{WF}^{out}=0 p.u., V_g=1 p.u., P_{WF}^{out}= 0.7 p.u. with equal power output from each WT. The total losses for this point are P_{WF}^{loss}=0.0032 p.u., which yields the losses gain, K_{loss}=0.9955.

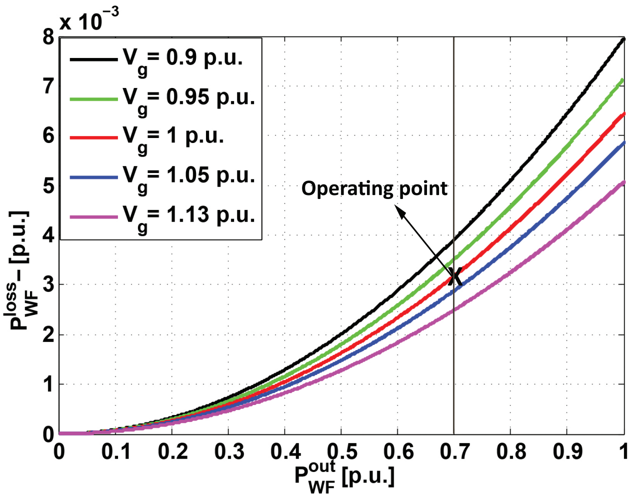

Figure 5.5. Operating point used for the design of the controller.

The value of the measured power in the PCC is not sent instantaneously to the controller. According to [2], a typical value of the delay,τ_m is 15 ms. This can be modelled as a first order system, with the following transfer function:

$$H(s) = \frac{1}{\tau_m s + 1} \tag{5.4}$$

In the following sections, the suitability and performance of the following controllers will be analysed:

- P-controller
- PI-controller with anti wind-up

5.3.1 Proportional Controller- P

The proportional controller has the transfer function:

$$G_c(s) = K_P \tag{5.5}$$

The closed loop transfer function of this plant can be determined by introducing Eq. 5.2 and Eq. 5.5 into Eq. 5.1, which yields:

$$\frac{P_{PCC}^{meas}(s)}{P_{PCC}^{ref}(s)} = \frac{K_P K_{loss}(\tau_m s + 1)}{\tau_P \tau_m s^2 + 1 + (\tau_p + \tau_m)s + 1 + K_P K_{loss}} \tag{5.6}$$

The steady state value of the closed loop with a P controller is:

$$P_{PCC}^{meas} = \lim_{s \to 0} G_{cl}(s) P_{PCC}^{ref} = \frac{K_P K_{loss}}{1 + K_P K_{loss}} P_{PCC}^{ref} \tag{5.7}$$

The steady-state error can be calculated:

$$err = \frac{1}{1 + K_P K_{loss}} \tag{5.8}$$

The proportional gain can be calculated based on the desired error relative to P_{PCC}^{ref}:

$$K_P = \frac{\frac{1}{err} - 1}{K_{loss}} \tag{5.9}$$

According to the grid codes the error should be less than 2% of P_n. To give a reasonable safety margin the desired error between the reference and the measured value is set to 1, 1.5 and 2 %, relative to P_{PCC}^{ref} and the behaviour for the different K_P gains is observed. The root locus of the closed loop poles can be seen in Figure 5.6 for different values of K_P.

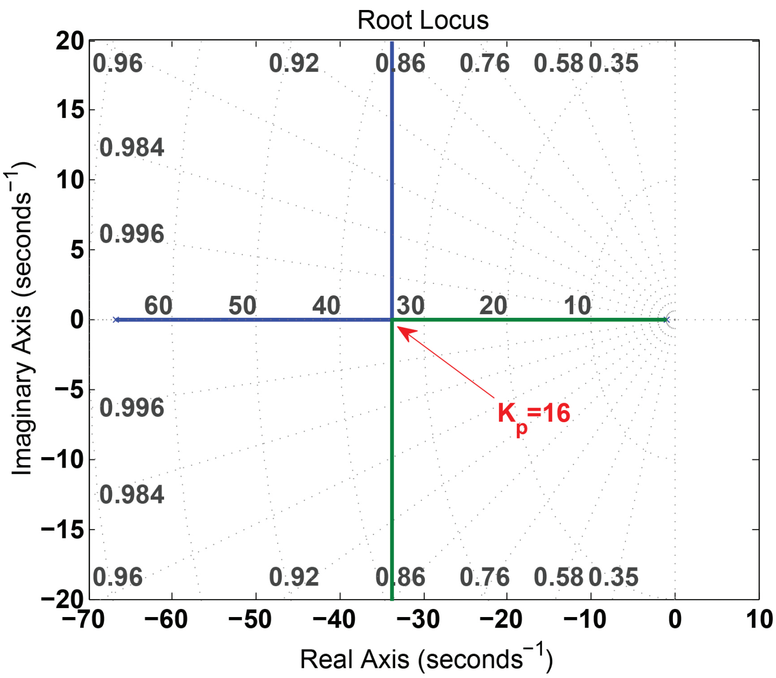

Figure 5.6. Root locus of the closed loop poles for different values of K_P.

For K_P>16 the poles are complex and the system will exhibit overshoot. The values of the overshoot for the different steady-state errors are presented in Table 5.3.1.

$Error$[%]	K_P	Overshoot [%]
1	99.4	24
1.5	66	15
2	49.2	10

Table 5.1. Overshoot for different values of maximum allowed error.

In order to verify if the overshoot is also occurring in the model a series of simulations has been carried out for two values of K_P. In these simulations it is desired to see the response to a demand from the TSO to change the power in the PCC by 0.1 p.u. The results are illustrated in Figure 5.7 and Figure 5.8.

When the reference from the TSO changes by 0.1 p.u. the reference in the PCC and to the turbines is limited by the ramp rate limit of the WTs, which as explained in Section 3.2 is set to 0.1 p.u./s. The controller output can therefore not change instantaneously, which explains the sawtooth profile. The steady state errors are -1% and -2% for K_P = 99.4 and K_P=49.2 respectively as expected. The overshoot is 14% and 6%, which is not acceptable. This leads to the need of a controller which can remove the overshoot and the steady-state error.

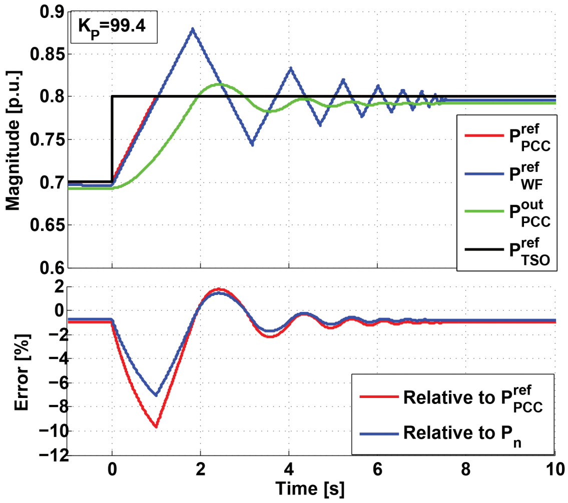

Figure 5.7. Simulated response of the active power in PCC to a step of 0.1 p.u. with K_P=99.4.

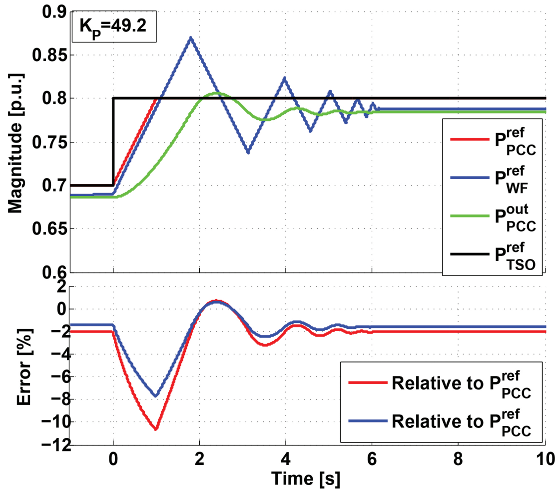

Figure 5.8. Simulated response of the active power in PCC to a step of 0.1 p.u. with K_P=49.2.

5.3.2 Proportional Integral Controller with Anti-windup- PI

The PI-controller is designed using the Modulus Optimum method. The method is based on replacing the slowest pole of the plant transfer function with a pole in the origin. This yields a result of the closed loop transfer function which has a response time similar to the response time of the plant [22] [23]. The transfer function of the PI-controller is:

$$G_c(s) = K_P \frac{T_i s + 1}{T_i s} \tag{5.10}$$

The controller has to replace the pole of the plant with the slowest time response, which in this case is the response time of the active power loop, with a pole in the origin:

$$T_i = \tau_P \tag{5.11}$$

K_P is selected as:

$$K_P = \frac{T_i}{K_{loss}} \tag{5.12}$$

To avoid that the integrator adds up error when the plant reaches its saturation an anti wind-up is added, which has the following reset gain [24].

$$K_R = \frac{1}{T_i} \tag{5.13}$$

The Bode plot of the open-loop, closed-loop and of the PI-controller can be seen in Figure 5.9. In the low frequency area the closed-loop exhibits the same behaviour, as the open-loop. The bandwidth of the closed-loop system is 1 rad/s. The phase margin is > 90° and the gain margin is well above 3, which indicates a stable system.

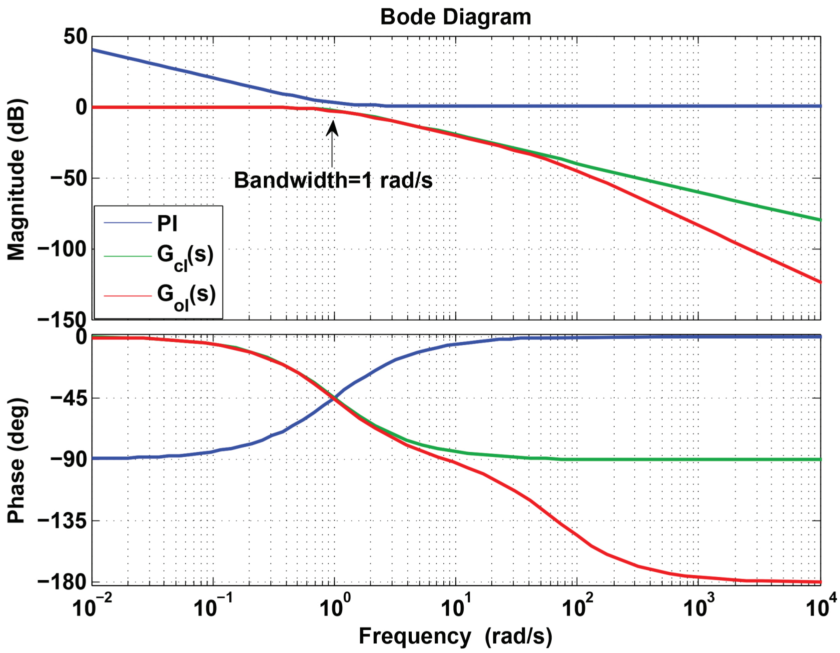

Figure 5.9. Bode plot of the controller, open loop and closed loop.

The poles of the closed loop system are placed in s_1=-65.6 s_2=-1.02 s_3=-1 so the system is stable and does not have any overshoot.
A simulation has been performed to observe the response to a demand from the TSO to change the power in the PCC by 0.1 p.u. The results can be seen in Figure 5.10. The settling time of the system is approximately 4.4 s, and there is no overshoot. The steady-state error is 0.

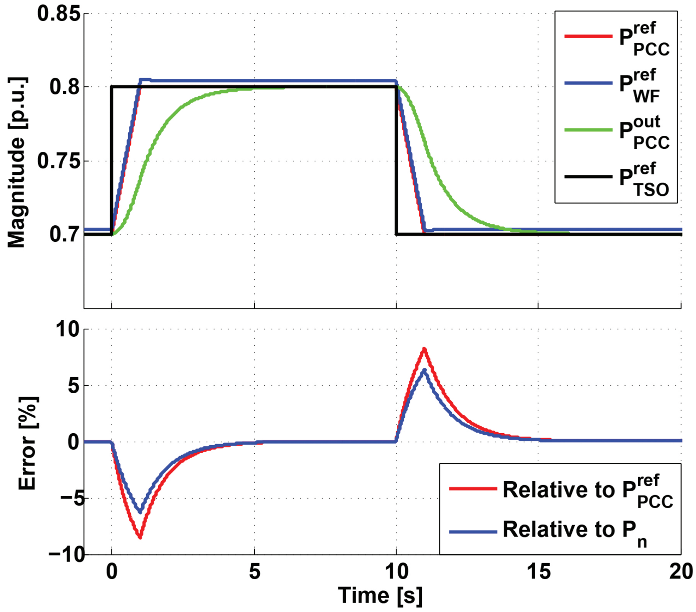

Figure 5.10. Simulated response of the power loop for $\Delta P^{ref}_{TSO} = \pm 0.1$ p.u. from 0.7 p.u.

5.3.2.1 Tuning of the PI-controller

The root locus method of tuning the PI is investigated. The closed loop poles of the system, when the gain of the controller is increased by a factor K can be seen in Figure 5.11.

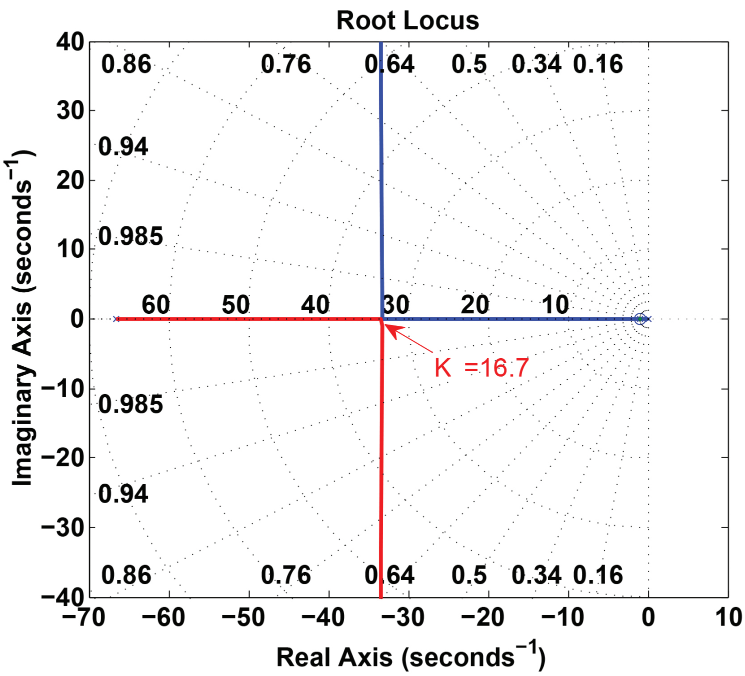

Figure 5.11. Root locus tuning of the PI-controller.

For K higher than 16.7 the system will exhibit overshoot. However, for gains higher than 1 the system will have a bandwidth higher than the bandwidth of the plant, which is not achievable. In addition to that the root locus method, does not take into account the saturation of the controller output. So, the gain K can have a value which is maximum 1. The minimum value of K, can be calculated using an iterative process. According to [21], the relationship between the settling time and bandwidth of the system is:

$$bw = \frac{4}{T_{set}} \tag{5.14}$$

For the investigated system, the bandwidth of the closed loop should be minimum 0.4 rad/s. From Figure 5.12, it can be seen that there is an almost linear relationship between the gain K and the bandwidth of the closed loop system. So the gain K can be minimum 0.4, if the settling time demand should be fulfilled.

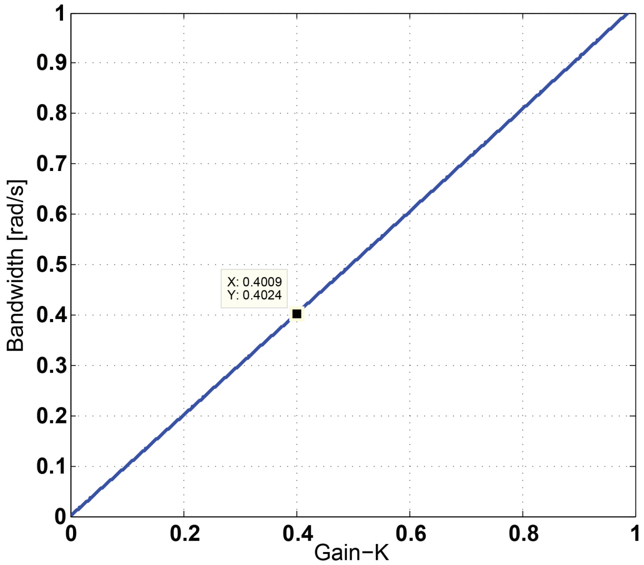

Figure 5.12. Bandwidth of the closed loop function as a function of the gain K.

The response of the closed loop system with K=0.4, for a step change of 0.1 p.u. is presented in Figure 5.13. There is no overshoot and the settling time is $\simeq$10 s as expected. The gain K should therefore be between $0.4 \leq K \leq 1$.

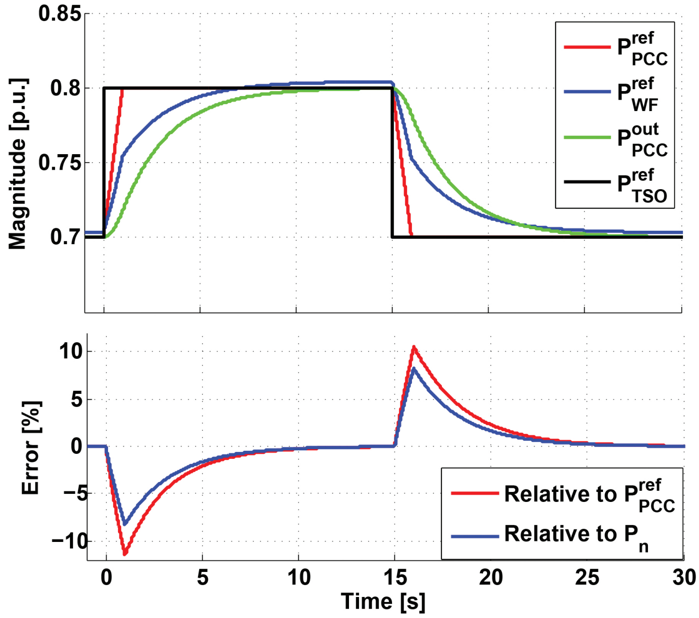

Figure 5.13. Simulated response of the power loop for $\Delta P_{TSO}^{ref} = \pm 0.1$ p.u. from 0.7 p.u. with K=0.4.

5.4 Verification of the Active Power Constraint Functions

The controller has been designed for a particular operating point. A series of simulations will therefore be performed to verify the robustness of the controller and its capability to reject disturbances in the entire operating range. The gain K is set to 1, since this will yield the fastest response. A step response of 0.1 p.u. for the following scenarios will therefore be investigated:

- Scenario 1. Fixed wind speed and equal dispatch.
  - Case 1. Different loading: 0.2 p.u. and 0.9 p.u.
  - Case 2. Different grid voltage: 0.9 p.u. and 1.13 p.u.
  - Case 3. Different SCR: 5 and 25
  - Case 4. Different XR: 5 and 20
  - Case 5. Different power factors: 0.96-ind and 0.98-cap
- Scenario 2. Varying and unequal wind speed including spacial delay.
  - Case 1. Wind from West
  - Case 2. Wind from North

5.4.1 Scenario 1. Fixed Wind Speed and Equal Dispatch

5.4.1.1 Case 1. Different Loading

In this set of simulations, it is desired to investigate the robustness of the controller for different loadings. The response to a step of 0.1 p.u. from 0.2 p.u. and 0.9 p.u respectively can be observed in Figure 5.14 and Figure 5.15. During these simulations the rest of the parameters have their standard values: V_g=1, SCR=10, XR=10, pf=1. For both cases the settling time is approximately 4.4 s and there is no overshoot. For the case presented in Figure 5.15, the steady state error is not zero, which is caused by the active power losses in the grid (maximum possible output power). It can also be observed, that the anti-windup functions properly, since the ramp-down is similar to ramp-up.

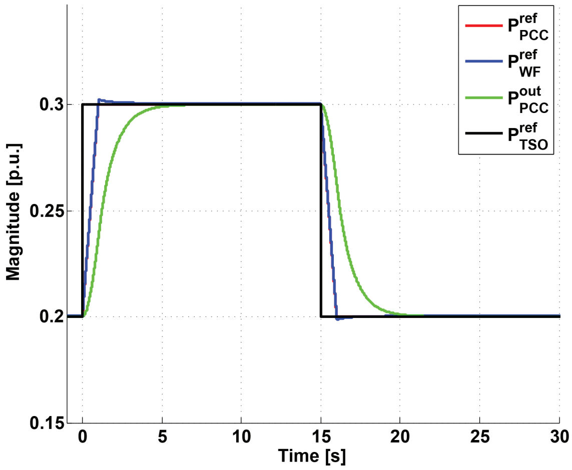

Figure 5.14. Simulated response of the active power in PCC to a step of 0.1 p.u. from 0.2 p.u.

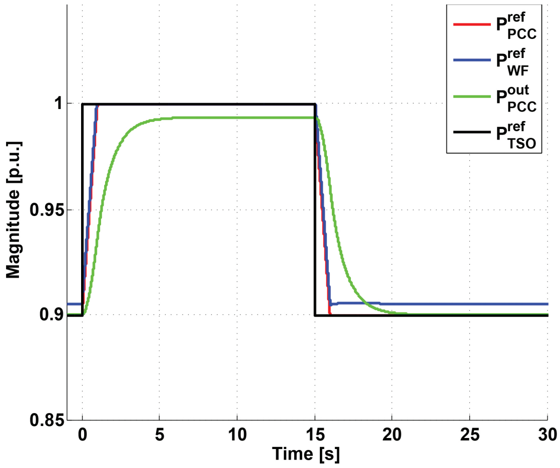

Figure 5.15. Simulated response of the active power in PCC to a step of 0.1 p.u. from 0.9 p.u.

5.4.1.2 Case 2. Different Grid Voltage

For this set of simulations the grid voltage is set to have values at the extremes, i.e. V_g=0.9 and V_g=1.13, with loading at 0.7 p.u., SCR=10, XR=10, and pf=1. The controller behaves as expected. The settling time is 4.4 s as in the previous case, there is no overshoot and the steady-state error is 0. For the lower grid voltage, i.e. V_g=0.9 the losses are higher compared to the higher grid voltage. This means that the reference sent to the WF also has to be higher (0.8052 p.u. compared to 0.8033 p.u.).

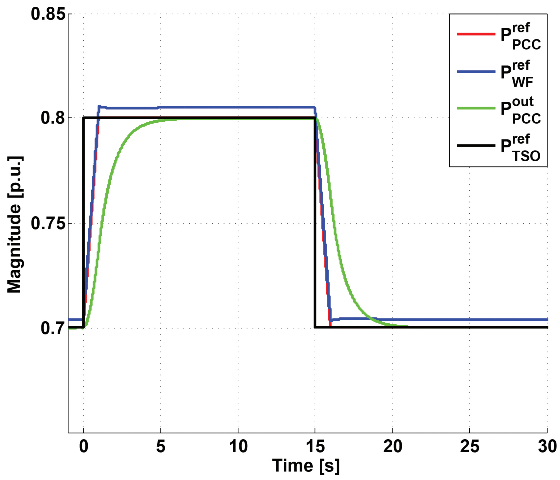

Figure 5.16. Simulated response of the active power in PCC to a step of 0.1 p.u. with V_g=0.9.

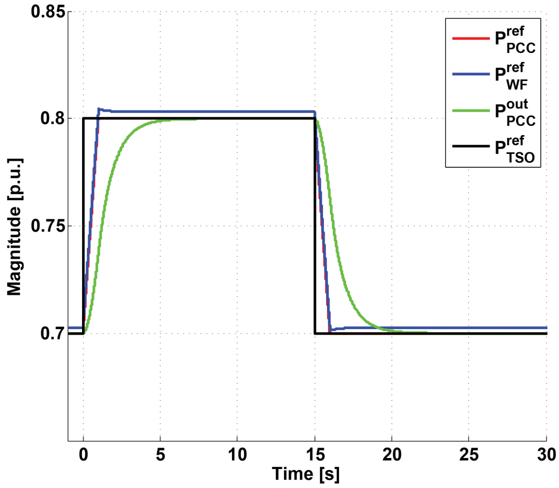

Figure 5.17. Simulated response of the active power in PCC to a step of 0.1 p.u. with V_g=1.13

5.4.1.3 Case 3. Different SCR

The impact of the SCR on the controller robustness is verified for two values: SCR=5 and SCR=25. The loading is set to 0.7 p.u., V_g=1, XR=10 and pf=1. The results can be seen in Figure 5.18 and Figure 5.19. The settling time is again 4.4 s, there is no overshoot and no steady-state error. There are no significant differences between the two cases and the base case. The controller is therefore good at rejecting the disturbance, which might originate from the inaccuracy in estimating the SCR.

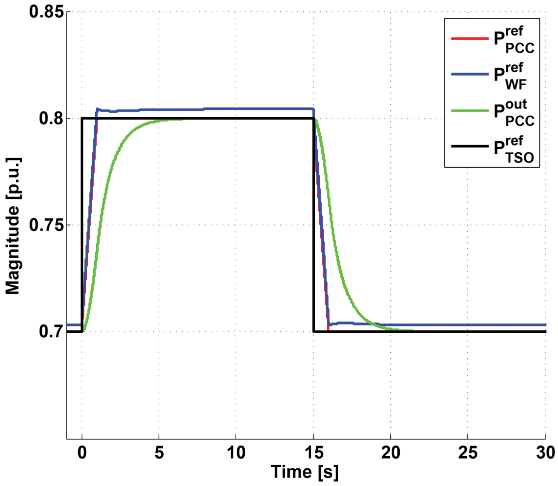

Figure 5.18. Simulated response of the active power in PCC to a step of 0.1 p.u. with SCR=5.

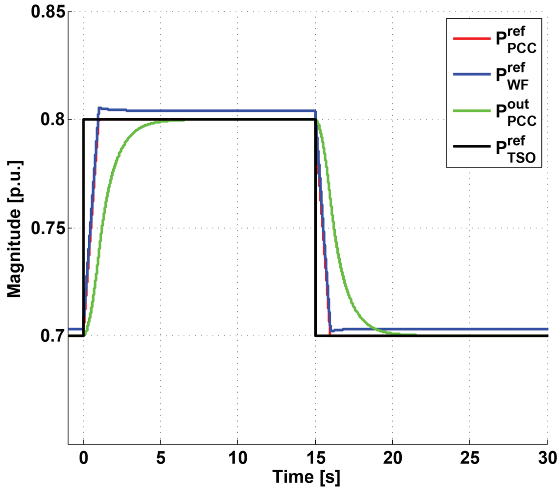

Figure 5.19. Simulated response of the active power in PCC to a step of 0.1 p.u. with SCR=25.

5.4.1.4 Case 4. Different XR

For this test case the influence of XR on the controller is verified for two values: XR=5 and XR=20. The loading is set to 0.7 p.u., V_g=1, SCR=10 and pf=1. The results of the simulation are illustrated in Figure 5.20 and Figure 5.21. The settling time is 4.4 s, there is no overshoot and steady-state error. The controller behaves as expected and is not affected significantly by the XR.

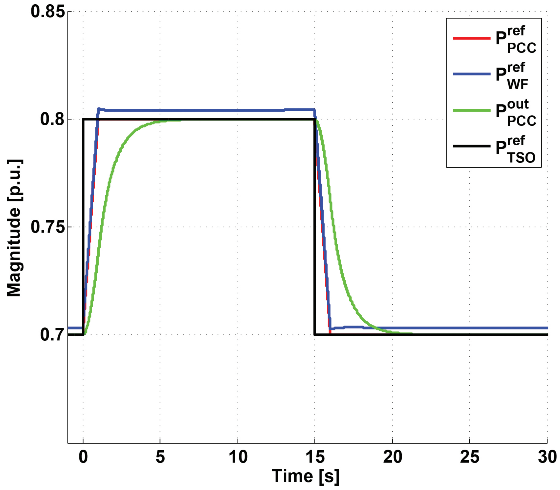

Figure 5.20. Simulated response of the active power in PCC to a step of 0.1 p.u. with XR=5.

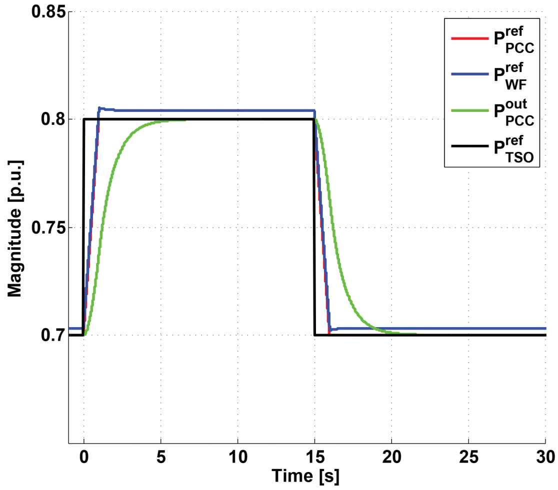

Figure 5.21. Simulated response of the active power in PCC to a step of 0.1 p.u. with XR=20.

5.4.1.5 Case 5. Different Power Factor

The impact of a non-unity power factor is investigated. The loading is set to 0.7 p.u, XR=10, SCR=10 and V_g=1. The results are presented in Figure 5.22 and Figure 5.23. The settling time is 4.4 s, there is no overshoot and the steady-state error is zero as in the previous test cases. Even though the WTs might produce power at non-unity power factor the controller is still able to track the reference and fulfil the requirements.

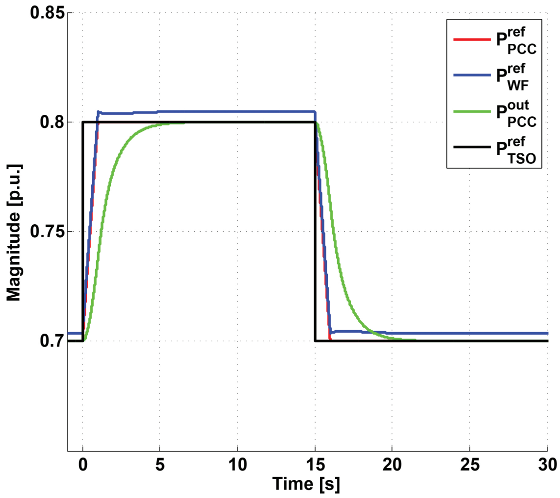

Figure 5.22. Simulated response of the active power in PCC to a step of 0.1 p.u. with pf=0.96-ind.

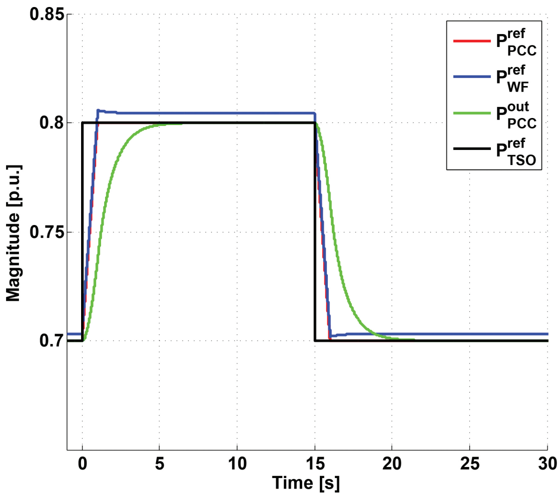

Figure 5.23. Simulated response of the active power in PCC to a step of 0.1 p.u. with pf=0.98-cap.

5.4.2 Scenario 2. Varying and Unequal Wind Speeds Including Spacial Delay

In this set of simulations the performance of the controller is investigated when the WTs experience different wind speeds. This is done in order to investigate the behaviour for conditions which are similar to the ones experienced in the field.

The layout of the WF is presented in Figure 5.24. The distance between the WT columns on the W-E direction is 500 m and the distance between the N-S rows is also 500 m. The columns are placed at 7° relative to the N-S axis.

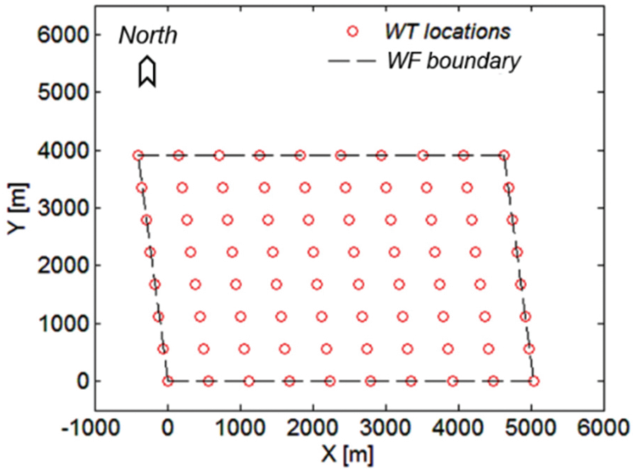

Figure 5.24. WT layout of the investigated WF. [25]

According to recordings taken at Esbjerg Airport, which is fairly close to the WF, the wind direction is primarily from West, see Figure 5.25 and Figure 5.26. Simulations will therefore be performed with the wind direction from West. In addition to that, simulations will also be performed for the cases when the wind direction is on the N-S axis. The turbulence intensity depends on the wind speed, but a value of 12% is very probable [26].
The wind used in the simulations is generated using the model presented in [28] and is

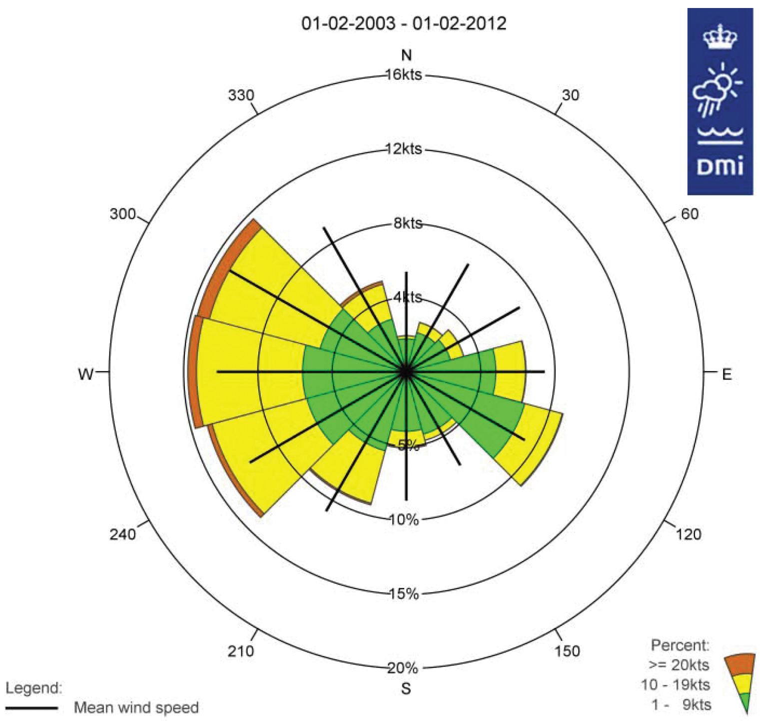

Figure 5.25. Wind rose at Esbjerg Airport during spring-summer (approx. 50 km from the WF.) [27]

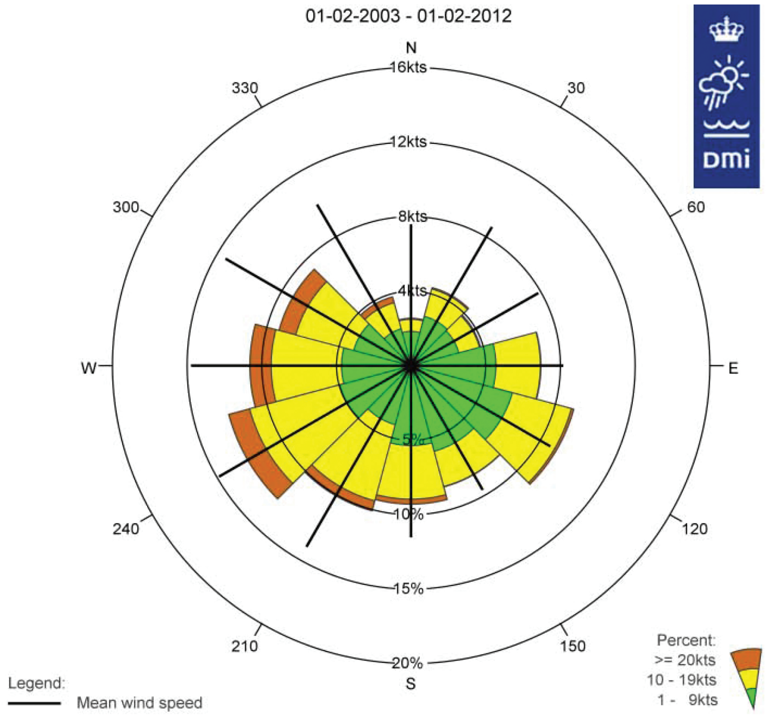

Figure 5.26. Wind rose at Esbjerg Airport during autumn-winter (approx. 50 km from the WF.) [27]

based on the Kaimal spectra. This wind model takes into account the tower shadow and rotational turbulences, based on the wing diameter and the WT rotational speed. The rotor rotational speed is obtained based on the average wind speed. According to [29], the rotor speed is a linear function of the average wind speed in the region, between the cut-off wind speed and the rated wind speed. At cut-in wind speed the rotor speed is 9 rpm and at rated wind speed and above the rotor speed is 16.7 rpm.
Only the wind experienced by the first WT in a row/column is generated, while the rest of the WTs experience the same wind with a variable time delay, which depends on the wind speed and the distance to the first WT.
The results of simulations which investigate the capability of the controller to perform the active power constraint functions demanded by the TSO are presented in the following subsections.

5.4.2.1 Simulation Results the Wind Direction from West and Equal Dispatch

For this case it is assumed that the wind direction is from West to East. The simulation is run with an average wind of 10 m/s and equal dispatch between the wind turbines. The investigated functions are performed according to the following time intervals:

- 0-200 s: Delta power constraint of 10% of the available power.
- 200-400 s: Maximum power point tracking.
- 400-1300 s: Ramp up and down from 0.5 p.u. loading with ramp of 0.000625 p.u./s (0.1 MW/s).
- 1300-1500 s: Ramp up and down from 0.5 p.u. loading with ramp of 0.1 p.u./s.

The response of the power in the PCC for different control functions is presented in Figure 5.27 a). In Figure 5.27 b), it can be observed how the time delay on the wind is successfully implemented (i.e. for a distance of approximately 5.5 km between WT_1 and WT_{80}, the wind is delayed by 522 s). In Figure 5.27 c) and 5.27 d) the power output of the same wind turbines is illustrated. The filtering effect of the rotor inertia can be noticed on the available power of each WT.

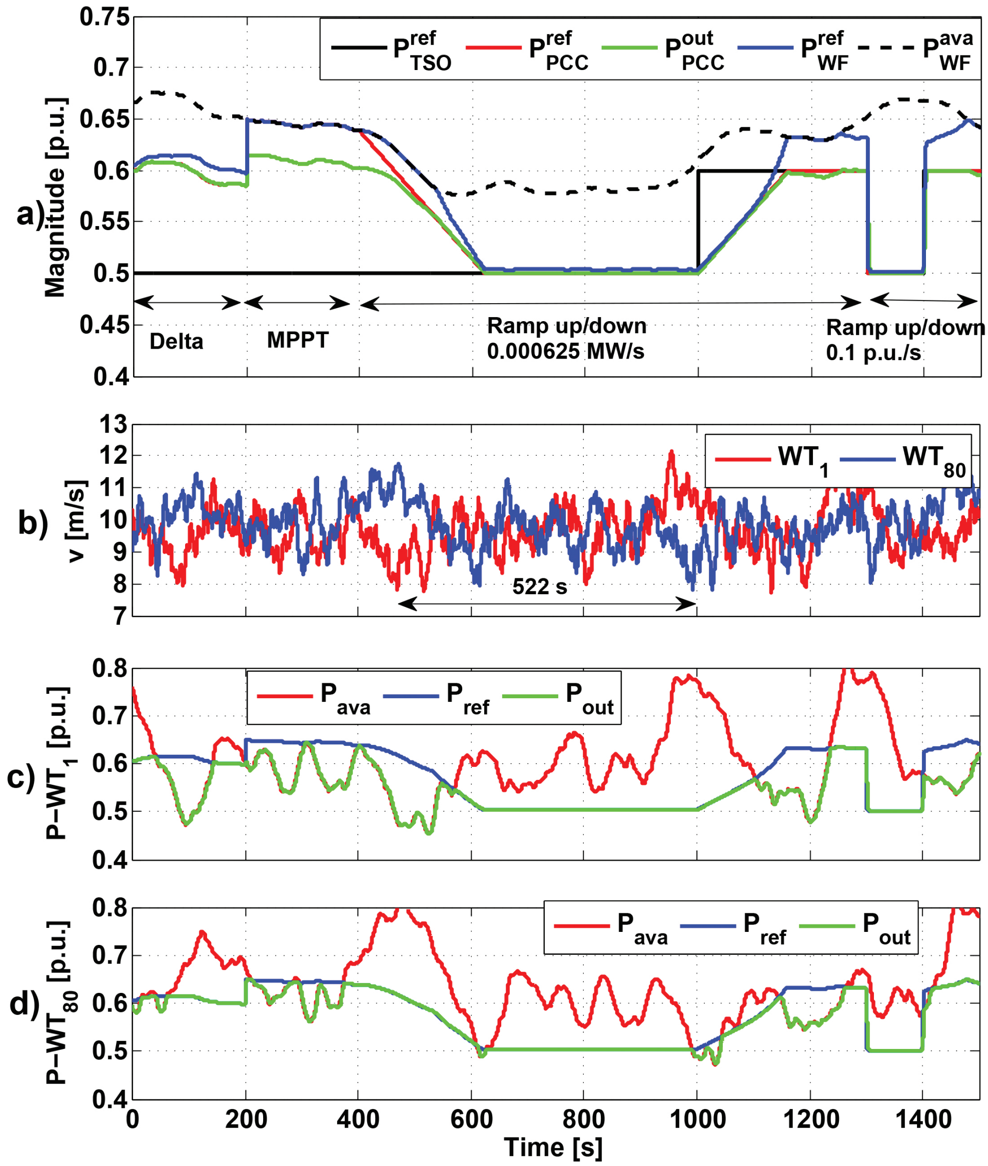

Figure 5.27. Simulation results for different control functionalities with v_{avg}= 10 m/s, equal dispatch and the wind direction is from West.

In the interval 0-200 s, the active power in the PCC, P^{out}_{PCC} is effectively controlled to be 10% lower than the total available power, P^{ava}_{WF} . In the interval between 200-400 s the MPPT is activated. This function does not function properly, since for some WTs the reference is lower than the available power, see Figure 5.28 at t$\simeq$300 s. At t=400 s, the WF is requested to perform a ramp down and then follow a reference of 0.5 p.u. until t=1000 s, which is performed well. At t=1000 s the WF is requested to ramp-up the power production and then keep the power constant at 0.6 p.u. until t=1300 s . The ramp up functions properly. However, at t≃1200 s the power in PCC does not track the reference longer, i.e. P_{PCC}^{out} is smaller than P_{PCC}^{ref}. This is not acceptable and it happens because the reference for some of the wind turbines is lower than the available power, as illustrated in Figure 5.28.

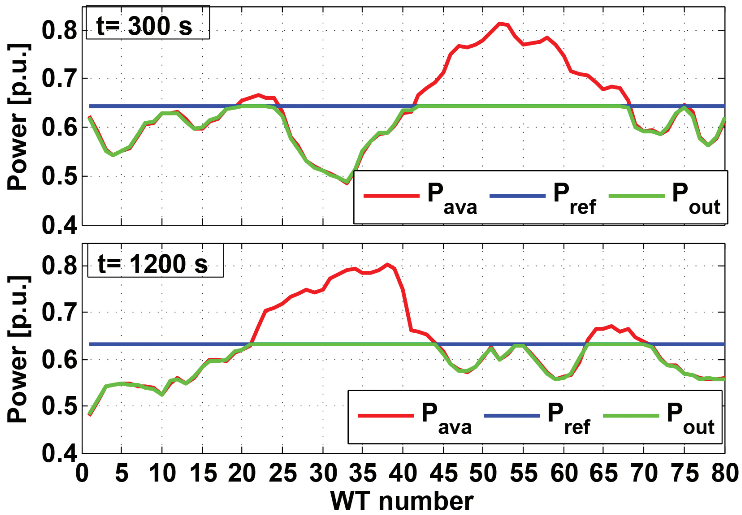

Figure 5.28. WT references, available powers and output powers at different simulation times for the equal dispatch test case.

Both the case when the output should follow the MPPT (t= 300 s) and at P_{PCC}^{ref}=0.6 p.u.(t= 1200 s) are presented. There is a great number of WTs that can deliver more power, but their capability is not used properly. This happens because P_{WF}^{ref} is limited to have a value lower or equal than the total available power (to avoid integrator wind-up), so for operating points close to the available power there will be cases when the power reference in the PCC can not be tracked. The proportional dispatch should remove the drawbacks of the equal dispatch and will therefore be investigated.

5.4.2.2 Simulation Results the Wind Direction from West and Proportional Dispatch

In this simulation the impact on changing the dispatch method from equal to proportional dispatch, as given by Eq. 2.2 is investigated. The same simulation conditions are applied as in the case of equal dispatch (i.e. v_{avg}=10 m/s, wind direction from West and the same order for the control functions.). The response of the active power loop in the PCC can be seen in Figure 5.29 a). The delta power constraint is successfully tracked between 0-200 s at 10% of the available power. A major improvement can be observed for the MPPT function (200-400 s), compared to the case with equal dispatch, since the output power is much closer to the available power. At t=400 the absolute power constraint is activated and the power is succesfully ramped down to 0.5 p.u., with the specified ramp. From t≃600 s to 1000 s, the power is kept constant at 0.5 p.u. At 1000 s the power is ramped up to 0.6 p.u. and is kept constant to that value. Between t=1300 s the power is ramped up and down successfully with the maximum ramp rate which can be tolerated (0.1 p.u./s). Figure 5.29 b) and Figure 5.29 c) illustrate the behaviours of WT_1 and WT_{80}. Here it can be seen that the references sent to the WTs are never higher than the available powers for these turbines.

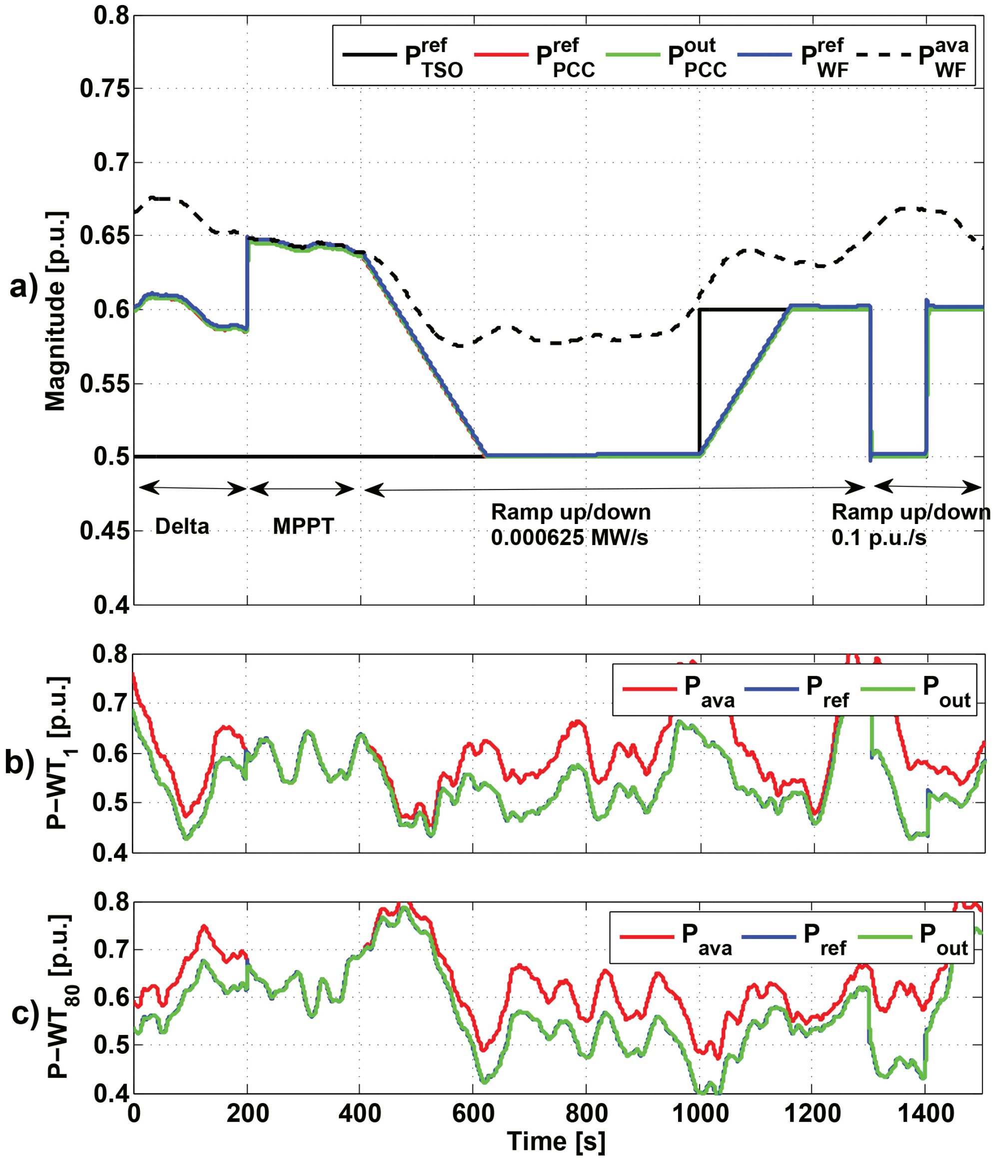

Figure 5.29. Simulation results for different control functionalities with v_{avg}= 10 m/s, proportional dispatch and the wind direction from West. In c) and d) P_{out} is on top of P_{ref}.

In Figure 5.30 the reference, available and output powers sent to the turbines at t=300 s (MPPT) and t=1200 s (absolute power constraint) are presented. During the MPPT period the references are equal to the available powers as needed and the output tracks the reference accurately. During the absolute power constraint period (t=1200 s), the WTs receive the proper references, which are never higher than the available power.
The superior performance of the proportional dispatch is confirmed based on the simulation results.

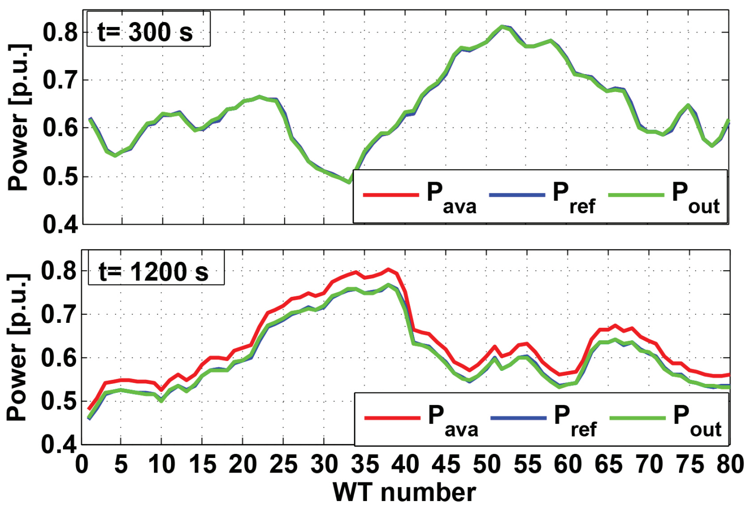

Figure 5.30. WT power references and available powers at different simulation times for the proportional dispatch test case. P_{out} tracks P_{ref} successfully for both cases.

5.4.2.3 Simulation Results with the Wind Direction from North and Proportional Dispatch

When the wind direction is from North, all the turbines in a row will experience the same wind. This is different from the case with the wind direction is from West, where each turbine experiences a different wind due to the 7° shift of the WTs with respect to the N-S axis. The same wind is used as for the case when the wind direction is from West. The results of the simulation are illustrated in Figure 5.31.

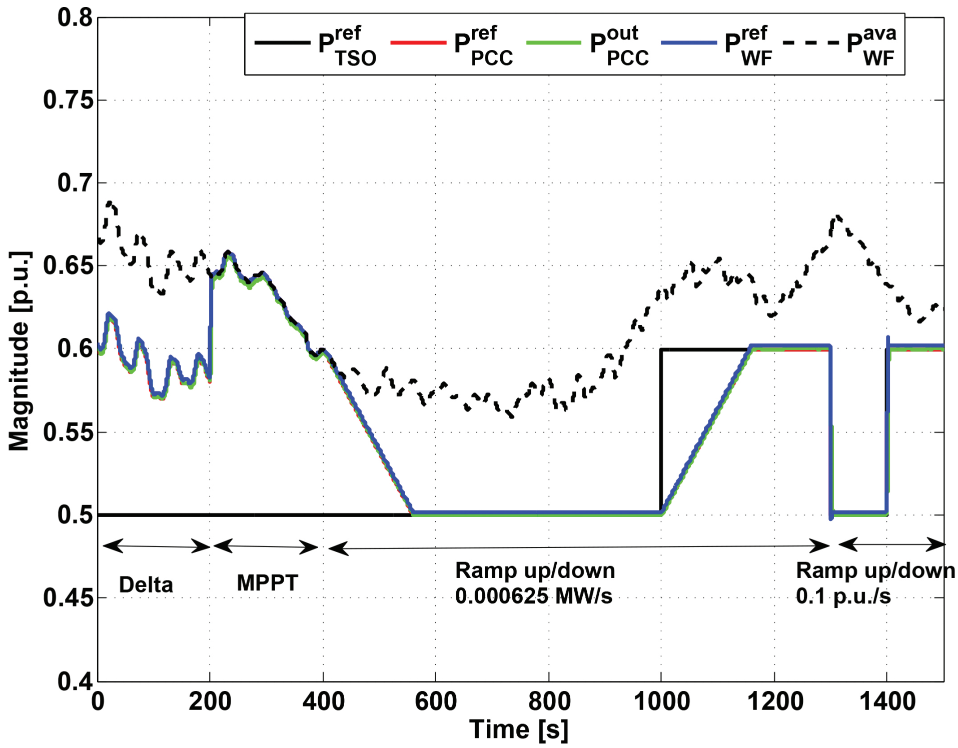

Figure 5.31. Simulation results for different control functionalities with v_{avg}= 10 m/s, proportional dispatch and the wind direction from North.

The controller is able to perform all the active power constraint functions properly. This case is worse than the case where the wind direction from West, due to higher oscillations in the available power. The difference in the available power oscillations can be shown using the power fluctuation index (PFI) [30]:

$$\Delta P_{WF}^{ava}(t) = \frac{P_{WF}^{ava}(t) - P_{WF}^{ava}(t - \Delta t)}{P_{WF}^{rated}} \cdot 100 \tag{5.15}$$

where Δt is the sampling time, and the time is taken at integer multiples of the sampling time. Figure 5.32 illustrates the available power and the PFI for different directions, with a sampling time of 1 s. It is clear that the case when the wind direction is from North is the worst case, where the PFI is up 0.32 in contrast to the case with the wind direction from West where the PFI is 0.07.

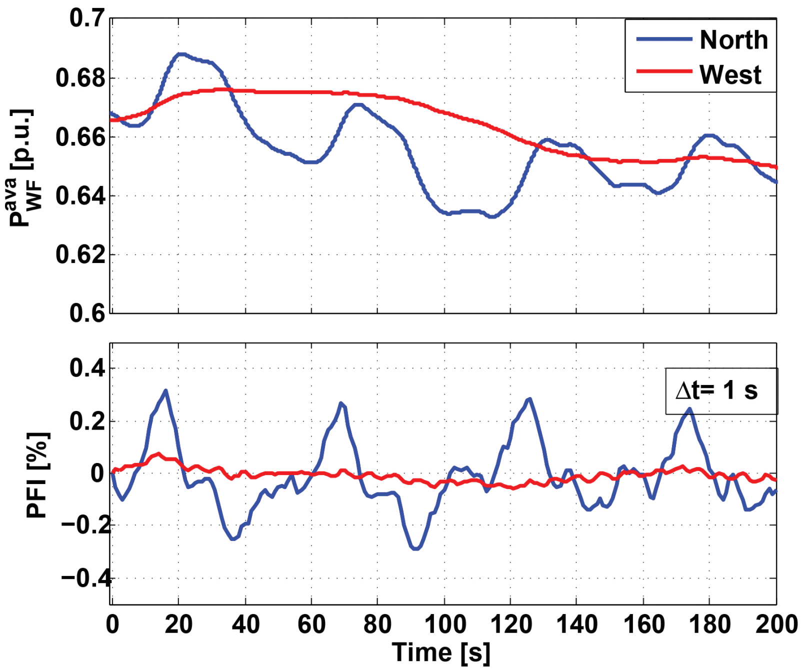

Figure 5.32. Available power and PFI for different wind directions.

5.5 Verification of the Frequency Control Functions

The capability of the controller to perform the frequency control functions presented in Section 5.1.1.2 is investigated in this section. The verification is made in a an open loop manner, which means that it will not be investigated how the power system stability is affected by the active power injected by the WPP. It will only be verified that the controller is able to send the correct active power output in the PCC in response to frequency changes in the grid. This is done assuming equal available power on all the turbines to make it clear that the curves required by the TSO can be tracked. The same average wind of 11 m/s is therefore supplied to all the turbines in order to make the results easy to interpret.

5.5.1 Frequency Response

In order to verify the frequency response capability, the frequency has been increased linearly from 50 Hz to 52 Hz. f_R has been set to 50.2 Hz and the droop to 4%. The results of the simulation are illustrated in Figure 5.33. The power in the PCC is reduced according to the specified droop when f exceeds 50.2 Hz. The frequency response has been successfully implemented.

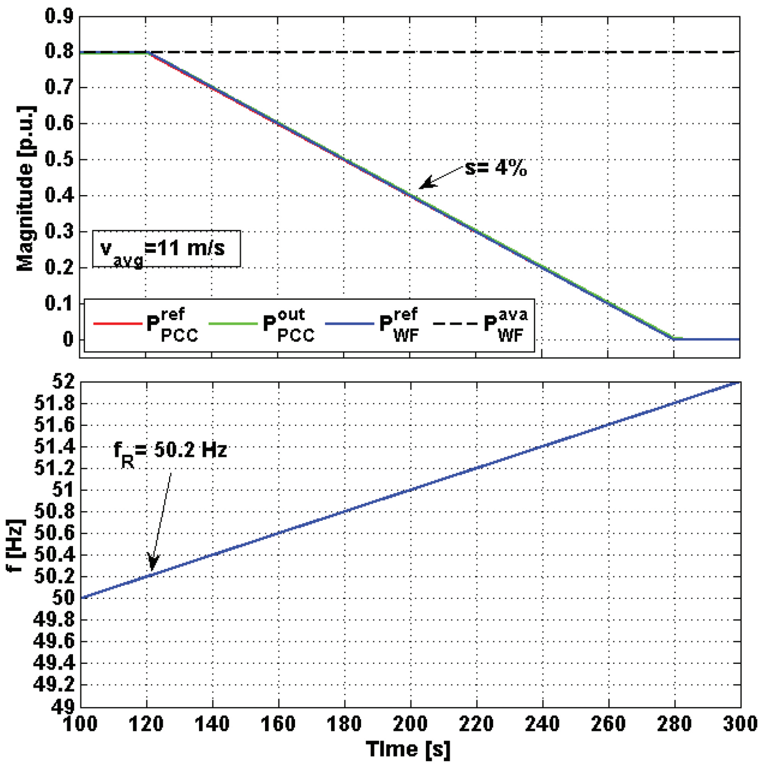

Figure 5.33. Frequency response functionality.

5.5.2 Frequency Control

The same approach as for the frequency response case was used to verify the frequency control. The major difference is that for this type of control it should be possible to specify different droops depending on the interval where the frequency lies. The results of the simulation are presented in Figure 5.34. As the frequency increases different droops are obtained, so this control function was also implemented successfully. When the frequency exceeds f_5, the ramp-up of the active power is not allowed until f drops bellow f_7. This function has been implemented using the 'State-Flow' toolbox from Matlab/Simulink. When f exceeds f_5 a flag is raised (i.e. the state is equal to 1) and is kept at 1 as long as f is higher than f_7. When the flag is raised a ramp-limiter block makes sure that the output power can not increase, but at the same time it allows for a decrease of the power output if the frequency is raised further. In order to prove that this function works properly, the frequency which simulates the measured frequency is increased linearly from 49 Hz to 52 Hz in the time interval 0-200 s and then decreased to 49 Hz again in the time interval 200-300 s as it can be seen in Figure 5.35.

The controller behaves as expected, i.e. when f increases above f_5 ramp-down is allowed

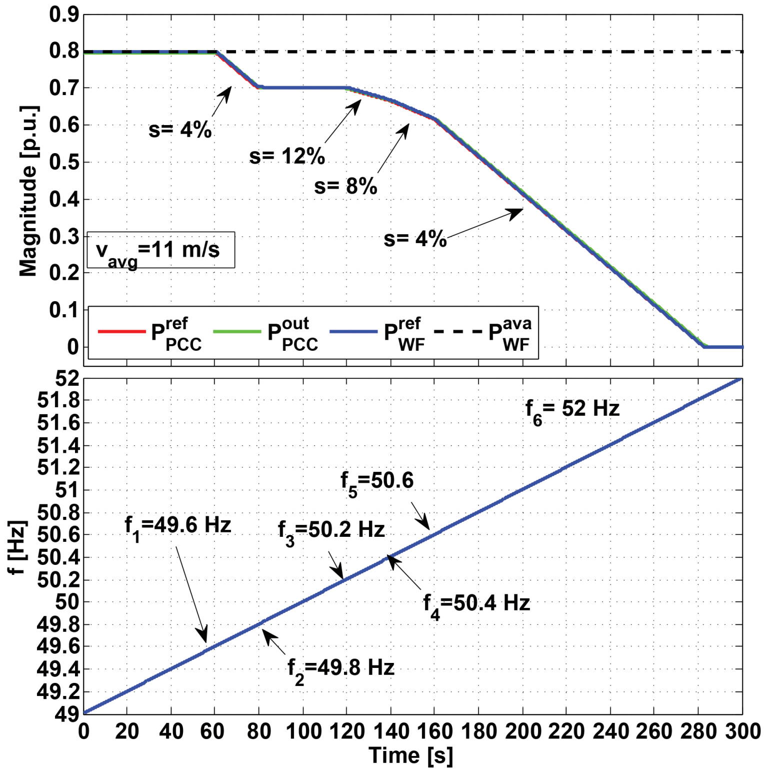

Figure 5.34. Frequency control functionality.

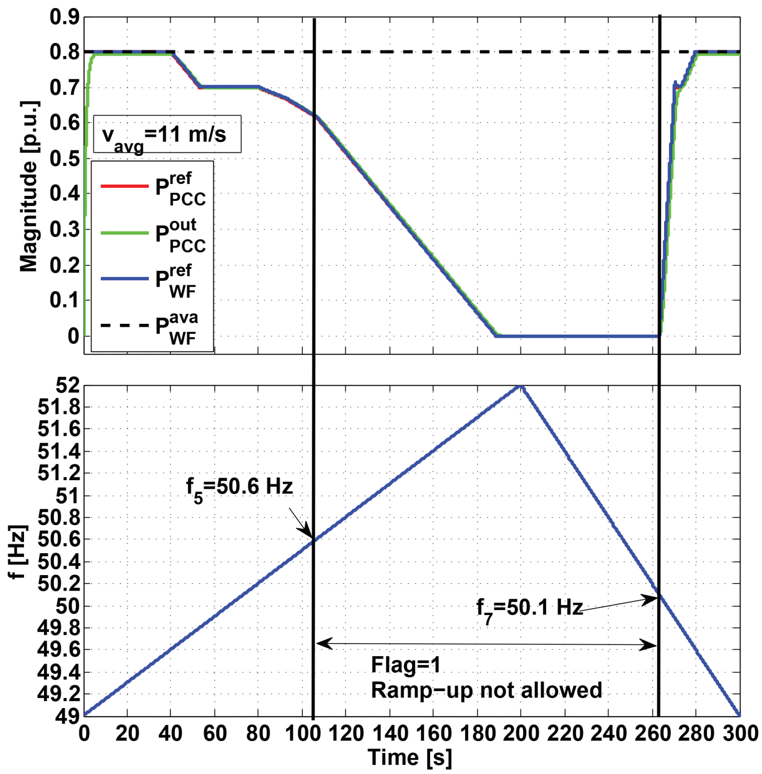

Figure 5.35. Frequency control for f above f_5.

and ramping-up is performed only when the frequency is lower than f_7.

5.6 Summary

An overview of the grid codes, which deal with active power and frequency control functionalities has been presented in the beginning of this chapter. These form the requirements of the controller that has to be designed. Two controllers have been investigated in the continuous time domain: P and PI. It has been concluded that the P controller is not suitable, since it can not fulfil the steady-state error requirement of 2 % without yielding an overshoot, if there is enough available power. The PI-controller has been designed at partial load using the modulus optimum criterion, which will yield a response of the closed loop similar to the response of the plant. In addition to that, the gain K which can be added to the PI-controller has been determine to be minimum 0.4 and still fulfil the settling time requirement of 10 s for 0.1 p.u. change. The gain K=1 has been chosen, since it yields the fastest response. Then the disturbance rejection capability of the controller has been verified for different parameters, such as SCR, XR, loading, etc. The controller still works as intended.
A set of simulations has been performed with different wind speeds on each turbine, with the wind direction from West and equal reference dispatch. It can be concluded that for points close to the available power, the controller is not able to regulate the power properly, since some of the WTs will produce less than their available power. For this reasons, the proportional reference dispatch has also been tested and it has shown a great improvement in the reference tracking capability. The methodology described here can therefore be used to develop the controller in the continuous time domain. In addition to the active power constraint functions, the frequency response and frequency control capability have also been verified successfully. For real WFs, the control is done in discrete time domain. In the next chapter it will therefore be investigated how the sampling time and the discretization method affects the robustness of the controller.

Considerations for Controller Implementation in Real-Time 6

The approach used to implement the controller and model in a RT-HIL environment is presented in this chapter. The first step is to investigate how the discretization of the controller affects the stability and performance of the system. The next step is to implement the model in OPAL-RT and run it off-line followed by running the model in RT. The final step is to include the hardware in the loop(i.e. Bachmann Controller), while the grid and the WTs are simulated in the RT environment.

6.1 Discretization of the Controller

The controllers implemented in WFs are usually discrete. It is therefore necessary to investigate how the sampling time and the discretization method affect the performance of the controller and the stability of the closed loop system. The diagram of a sampled system, using a digital controller can be seen in Figure 6.1. The error between the reference and the measured value is sampled with 0.1 to 1 s. In [6] it is mentioned that the sampling time, T_s of the WFC should be done with a maximum of 10 s. This value is to high and it would not allow a settling time of 10 s, so the design of the controller should be done for a sampling time of 1 s.

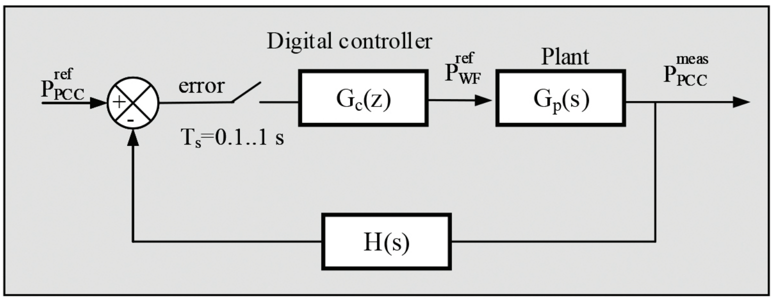

Figure 6.1. The closed loop diagram of the discrete system.

6.1.1 Investigation on the impact of discretization

The transformation of the controller from the continuous domain to the discrete time domain can be done using different approaches. The most used discretization method are presented in Table 6.1.1, where the s-terms are replaced by the appropriate z-functions.

With Forward Euler transformation a stable system in s-domain might be mapped into an unstable system in the z-domain. Both the Backward and Tustin maintain the stability of the system when mapping from s- to the z-domain.

Forward Euler	Backward Euler	Tustin
$s = \frac{z-1}{T_s}$	$s = \frac{z-1}{T_s z}$	$s = \frac{2}{T_s}\left(\frac{z-1}{z+1}\right)$

Table 6.1. Discretization methods. [21]

The transfer function of the PI-controller in the z-domain in canonical form can be expressed as:

$$G_{PI}(z) = \frac{b_0 + b_1 z^{-1}}{1 - a_1 z^{-1}} \tag{6.1}$$

with the parameters a_1, b_0, and b_1 depending on the discretization method, as summarized in the following table:

Parameter	Forward Euler	Backward Euler	Tustin
a_1	1	1	1
b_0	K_P	$K_P + \frac{K_P T_s}{T_i}$	$K_P(\frac{T_s}{2T_i} + 1)$
b_1	$\frac{K_P T_s}{T_i} - K_P$	$-K_P$	$K_P(\frac{T_s}{2T_i} - 1)$

Table 6.2. Parameters of the discrete PI-controller.

The block diagram of the discrete PI expressed in the canonical form is illustrated in Figure 6.2.

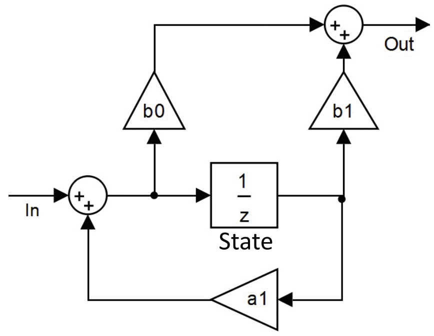

Figure 6.2. Block diagram of the discrete PI-controller expressed in canonical form.

The output of the controller can therefore be expressed as:

$$Out = b_0 \cdot In + b_0 \cdot a_1 \cdot State + b_1 \cdot State \tag{6.2}$$

The state is updated using:

$$State = a_1 \cdot State + In \tag{6.3}$$

An alternative method to express the discrete controller is using difference equations:

$$Out(k) = a_1 \cdot Out(k-1) + b_0 \cdot In(k) + b_1 \cdot In(k-1) \tag{6.4}$$

where k is the current time step and $k-1$ denotes the previous time step.
The implementation is illustrated in Figure 6.3, where additional blocks such as the ramp rate constraint and the gain, K are included. The main advantage of expressing the controller in this format is the easiness to implement the anti-windup.

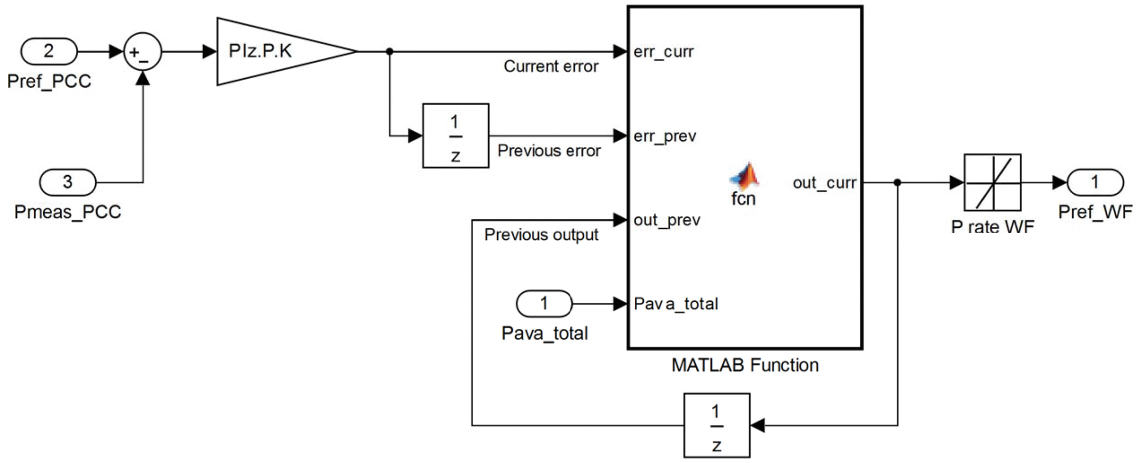

Figure 6.3. Discrete PI-controller with anti wind-up.

The code for generating the controller output with the anti-windup is presented in Figure 6.4.

```
function out_curr = fcn(err_curr, err_prev, out_prev, PIz_P_a1, PIz_P_b0, PIz_P_b1,
Pava_total)
%#codegen
out_curr=PIz_P_a1*out_prev+PIz_P_b0*err_curr+PIz_P_b1*err_prev;
if out_curr>Pava_total
   out_curr=Pava_total;
   else
       out_curr=out_curr;
end
out_curr=max(0,out_curr);
end
```

Figure 6.4. Code used to generate the controller output.

The sampling time has a significant impact on the response and stability of the system. In order to see the impact of the sampling time, simulations are performed with equal dispatch and with the available power equal to the rated power of the WF. K_P and T_i are the same as for the continuous system, described in Section 5.3.2 and K=1. The difference between the continuous and discrete time response, where different discretization methods were used (i.e. Backward Euler and Tustin), is illustrated in Figure 6.5 and Figure 6.6. For low sampling times, e.g. 0.1 s the response of the discrete system is similar to the response of continuous system. When the sampling time is increased to 1 s the discrete system exhibits a significant overshoot disregarding of the discretization method, assuming that there is enough available power to allow the overshoot.

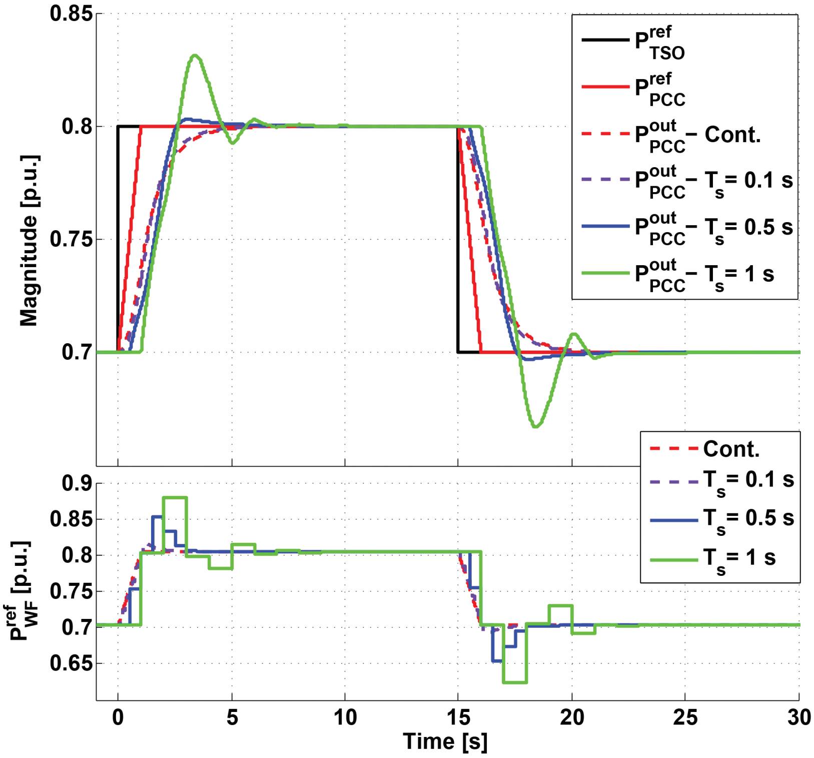

Figure 6.5. Comparison between the closed loop step response of the continuous and discrete system (Backward Euler) with different sampling times.

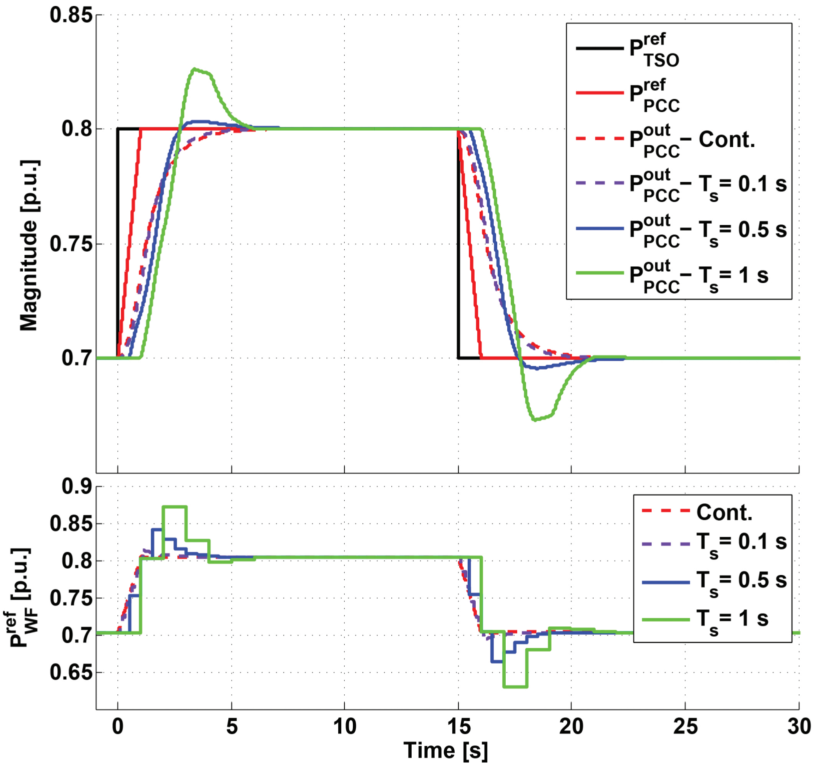

Figure 6.6. Comparison between the closed loop step response of the continuous and discrete system (Tustin) with different sampling times.

In Section 5.3.2 it has been shown that the system is still able to meet the requirements

even though the gain of the PI-controller is reduced with a gain K of 0.4. This reduces the bandwidth of the system and should also eliminate the overshoot. So a new set of simulations is performed with a sampling time of 1 s and the gain K= 0.4.
Figure 6.7 and Figure 6.8 illustrate the response of the system with the gain K reduced to 0.4. The system using the Tustin discretization has a settling time of 8.2 s, while Backward Euler has a settling time of 10 s. Both discretization methods fulfil the requirements, since they have no overshoot, zero steady-state error and settling time lower than 10 s.

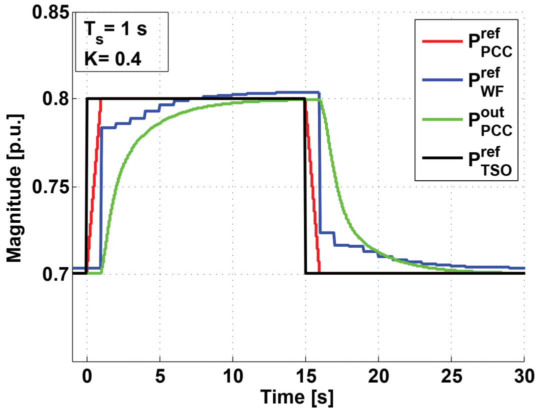

Figure 6.7. Simulated response with Backward Euler discretization and K=0.4.

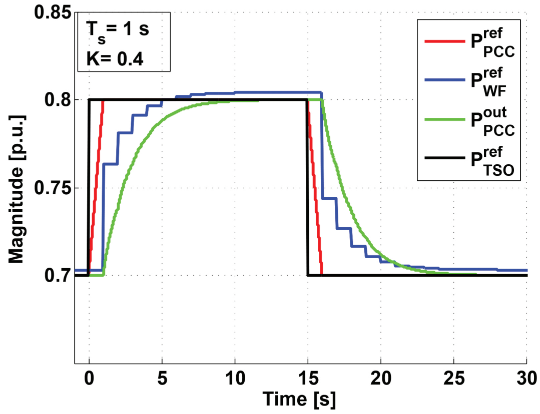

Figure 6.8. Simulated response with Tustin discretization and K=0.4.

6.1.2 Varying Wind Speeds With the Wind Direction from North and Proportional Dispatch

In this subsection it will be verified if the controller is able to maintain the stability and performance when the WTs experience different winds. In the previous section it has been proven that the worst case is when the wind direction from North, since more WTs experience the same wind. In addition to that, it was also shown that the equal dispatch does not work, so the proportional dispatch will be used. Even though the continuous system meets the requirements for a gain K=1, the discrete system exhibits overshoot. The gain K was therefore chosen to be K=0.4, and the fastest response was obtained using the Tustin discretization method. A simulation will therefore be performed using the setup described in this paragraph. The results are displayed in Figure 6.9. The controller is able to track the reference and performs all the active power constraint functions demanded by the TSO.

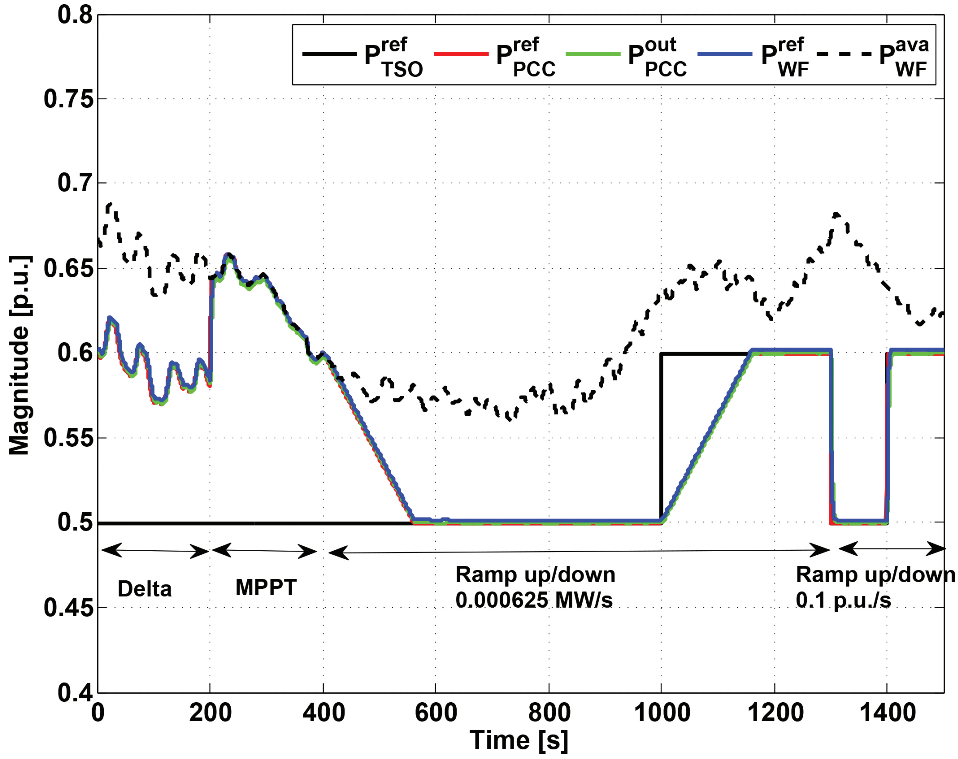

Figure 6.9. Simulation results using the Tustin discretization method, wind direction from North and proportional dispatch.

For better clarity a zoom is presented in Figure 6.10 and here it can be observed that the settling time is approximately 10 s as expected, there is no overshoot and no steady-state error.

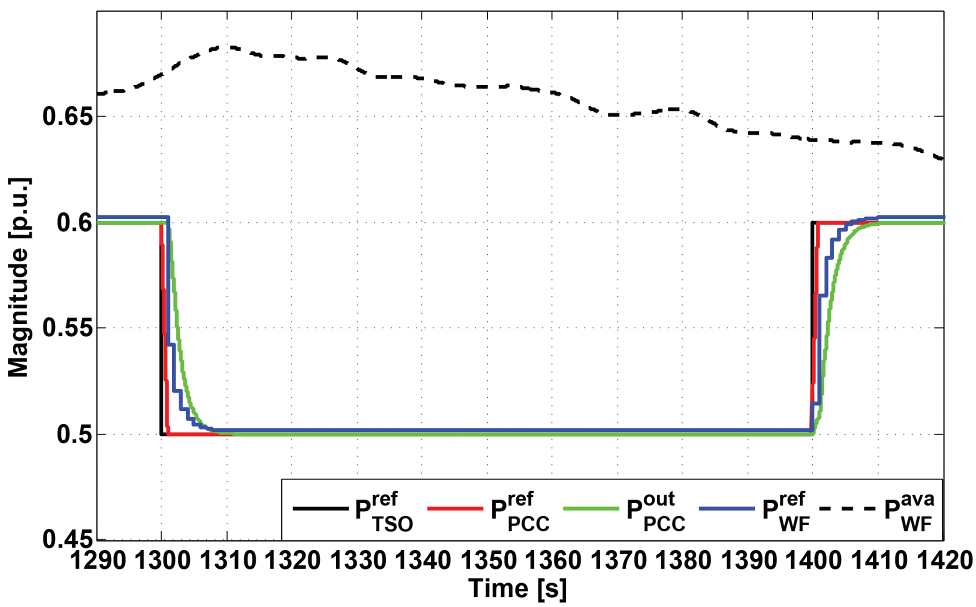

Figure 6.10. Zoom of Figure 6.9 in the interval 1290-1420 s.

6.2 Model Implementation in Real-Time Environment

The implementation of the system in OPAL RT-HIL is made using the set-up described in `http://www.et.aau.dk/department/laboratory-facilities/smart-energy-systems-lab/` and the system has also been used for the voltage control in a WF [31]. The OPAL-RT system has 2 CPUs and there are 4 cores on each CPU. The computation of different subsystems can be assigned to each core. The model is therefore rearranged to allow the distribution of the computation tasks if one core is not enough. The top-layer of the model must only contain subsystems. One or multiple subsystems can be used for the computation in RT and one subsystem is allocated for the graphical user interface (GUI), where the setpoints can be changed and data can be visualized. The top layer of the Simulink model is presented in Figure 6.11. The subsystem $SM\_computation$ is used for the computation and subsystem SM_GUI is the console (GUI). In order to keep the interface simple, some parameters such as droops and frequency settings are initiated and can not be changed on-line.

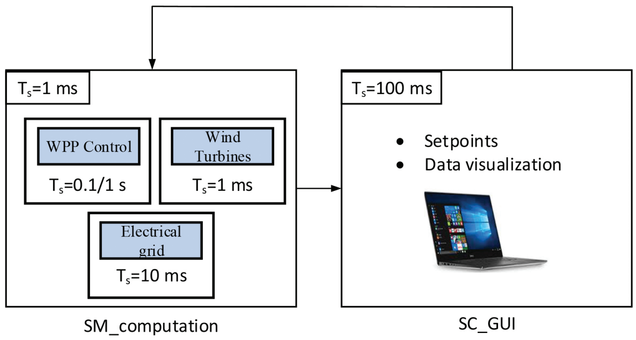

Figure 6.11. Top layer of the Simulink model.

The computation subsystem performs the calculation with a step size of 1 ms and is divided into three major parts:

- Main Controller- contains all the control functionalities and sends the references to the wind turbines. Two sampling times are investigated for this block: 100 ms and 1 s.
- Wind Turbines- this block contains the calculation of the available power for each turbine and it sends the current reference for the current source which injects power in the bus where the WT is connected. The sampling time of this block is 1 ms.
- Electrical Grid- it contains the electrical grid and measurements related to it. The electrical grid is implemented using the ePhasor module from OPAL-RT, which can support up to 10000 RMS buses. Sampling and calculations are made with 10 ms.

The data acquisition is also made in the computation subsystem with a sampling time of 100 ms. Visualization of the data is also done with a sampling time of 100 ms in the GUI subsystem. The implementation of the model in OPAL-RT is presented in Figure 6.12. All the computations are made on 1 core, but due to the modular form of the model the tasks can be divided to multiple cores if there are occurring overruns.

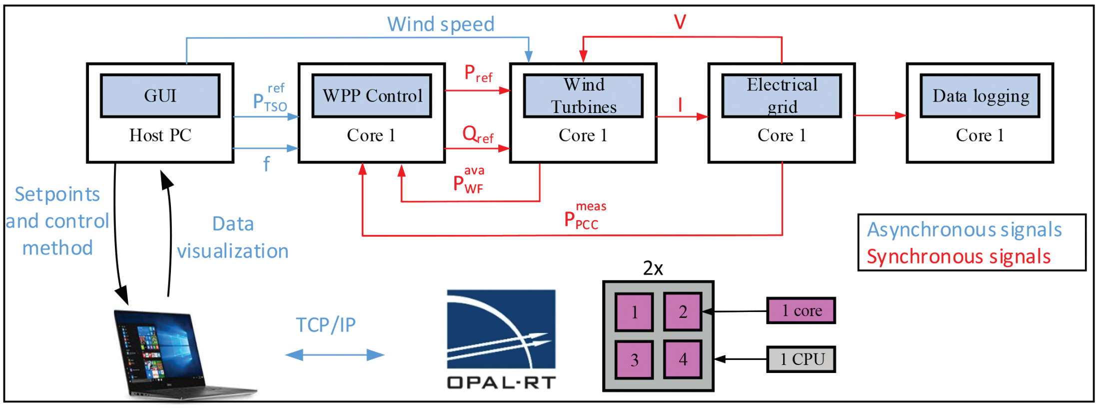

Figure 6.12. Implementation of the model in OPAL-RT.

6.2.1 Real-Time Simulation Results

The model has been successfully implemented in Real-Time and a series of simulations have been performed to investigate the controller functionality and if there are major changes compared to the off-line simulations. This is a necessary step before adding the Bachmann controller (hardware) in the loop. The step response for different discretization methods and controller sampling times is illustrated in Figure 6.13 and Figure 6.14. For a sampling time of 0.1 s, there is no significant difference between the Backward Euler and the Tustin discretization methods and the settling time of the system is 10 s. For a sampling time of 1 s, the Backward Euler method yields a settling time of 10 s and the Tustin method yields a settling time of 8 s. All these results are similar to the results obtained during off-line simulations.

Contacts from the industry suggested that in most of the modern WFs the control is done

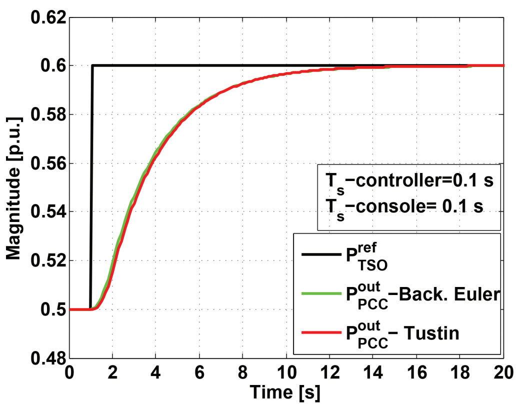

Figure 6.13. System response in Real-Time for T_s-controller= 0.1 s.

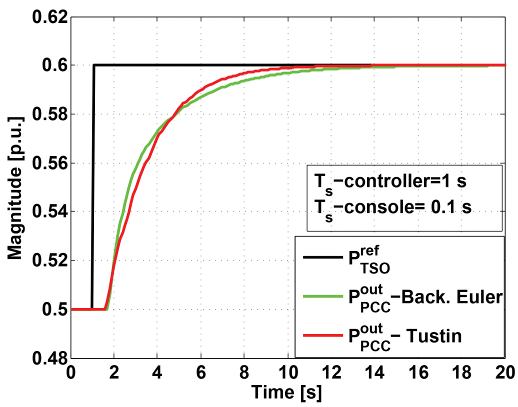

Figure 6.14. System response in Real-Time for T_s-controller= 1 s.

with a sampling time of 0.1 s. This is primarily done to meet reactive power requirements. The Tustin method yields the fastest response, so the active power control functionalities are verified using this method and a controller sampling time of 0.1 s. Results of a simulation where the delta-constraint and ramp rate constraint capability are investigated are presented in Figure 6.15. Initially the controller is set to MPPT and at t=8 s the controller is demanded to change the control strategy and keep a spinning reserve of 10 % of the available power. The ramp rate during this transition has the maximum value i.e. 0.1 p.u./s. The delta constraint works properly, e.g. at t= 26 s, the output power is ≃0.6 p.u., which is ≃10% lower than the available power, i.e. 0.66 p.u. At t= 38 s, a transition to MPPT is requested, but this time with a ramp rate limit of 0.01 p.u./s. It can be observed that this control function also works properly in RT.

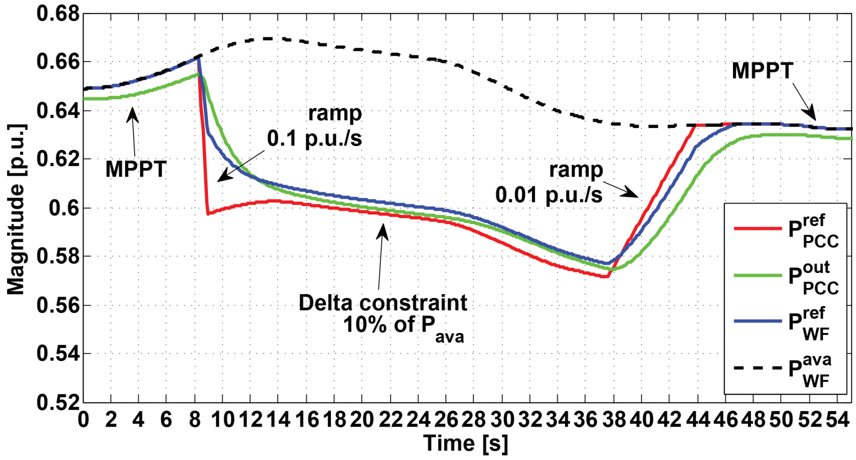

Figure 6.15. Active power constraint functionalities with T_s-controller=0.1 s and Tustin discretization.

The frequency response capability has been investigated in RT by gradually increasing the frequency from the console and observing the active power output of the WF. This functions also works properly. According to the droop setting of 4%, at f=50.6 Hz, the spinning reserve, ΔP should be $\Delta P = \frac{1}{0.04}\frac{0.4}{50} = 0.2$ p.u., which is also the case for the simulation, see Figure 6.16 at t=55.1 s.

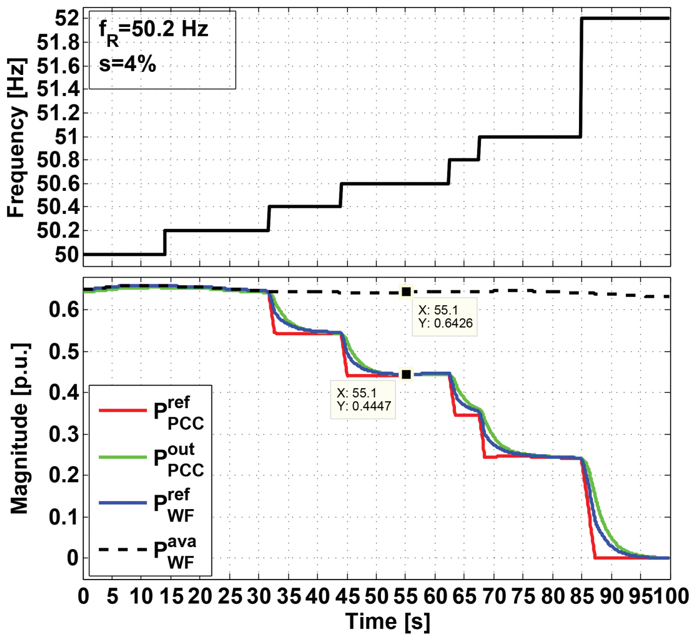

Figure 6.16. Frequency response capability.

6.3 Summary

The impact of the controller sampling time and discretization method on the stability and performance of the system has been investigated in this chapter. It has been shown, that for a sampling time of 0.1 s the system response is similar to the case where a continuous controller has been implemented. When the sampling time is increased to 1 s, the system exhibits overshoot and it is therefore necessary to reduce the bandwidth, by adjusting the tuning gain K to 0.4. With this new settings the controller meets al the requirements disregarding of the sampling time and discretization method. The model has been implemented in a RT environment and simulations were performed to verify all the active power functionalities required by the grid codes. The robustness of the controller is maintained in RT also and the results are similar to the results obtained when the controller was running off-line.

Discussion and Conclusion 7

This project has been carried out in collaboration with Vattenfall. The company desires to develop their own Wind Farm Controller(WFC) for the reasons stated in the problem statement. The aim of this project is to design and tune a WFC with focus on active power and frequency control.
The following objective were set in the begging of the project:

1. Develop a controller which can perform active power and frequency control functionalities in the Point of Common Coupling (PCC), with requirements originating from the grid codes.
2. Implement an appropriate dispatch function.
3. Verify the robustness of the controller through simulations.
4. Validation of the controller in a Real Time Hardware in the Loop (RT-HIL).

The design of the controller is made based on requirements originating from the Danish grid codes. An offshore wind farm placed on the West coast of Denmark, rated at 160 MW, which consists of 80 wind turbines is chosen to test the functionalities of the controller. A model of the WF is implemented in Simulink. The steady-state behaviour of the model is compared with results obtained from a commercial power systems tool. The deviation in the bus voltages is less than 0.3% and the deviation in active power losses in the grid is maximum 1.61%. The results have an acceptable deviation, so the Simulink model is used to investigate the influence of certain parameters (i.e. short circuit ratio, XR ratio, voltage of the external grid, WF power output and power factor) on the grid losses. This has been done to obtain a simplified version of the plant transfer function.
To fulfil the grid codes, the controller must yield the following results:

- Stable system
- No overshoot
- Steady-state error $<$2% of P_n
- Settling time $<$10 s for a step change of 0.1 p.u./s

Two different controllers have been investigated, P and PI. The P controller is designed based on a steady-state error criteria. It is however not capable to meet the requirements, since it yields overshoot and steady-state error. The PI has been designed in the s-domain using the Modulus Optimum criteria and tuned based on the requirement of settling time. An antiwindup is also implemented to limit the output of the controller at the availble power of the wind farm. The robustness of the PI-controller has been verified successfully, for different values of the SCR, XR ratio, external grid voltage loading and power factor. In addition to that, different scenarios have been carried out, where the WTs have different available powers and different wind directions. When equal reference dispatch is sent to

the WTs, the controller does not work properly for operating points close to the available power. A more suitable dispatch is chosen, which sends references to the turbine based on their available powers. This method is considerably better. The controller can function properly in the entire operating range and performs all the functionalities needed by the grid codes: active power constraint, delta constraint, ramp rate constraint, frequency response and frequency control. With a bandwidth of 1 rad/s, the system also has a settling time lower than 10 s.
Control of the WFs is made in discrete steps so it is also investigated how the discretization method and the sampling time influences the performance of the controller. For a sampling time of 100 ms, the response of the controller is similar to the response in continuous time domain, disregarding of the discretization method. For a sampling time of 1 s, the system starts to exhibit a significant overshoot. The bandwidth of the system needs to be reduced to a maximum 0.4 rad/s, to maintain the settling of <10 s. With this bandwidth and a sampling time of 1 s, settling times of 10 s and 8.2 s are obtained for the Backward Euler method and Tustin method respectively.
As a final step, the system has been implemented succesfully in a Real-Time Enviroment, with results similar to the ones obtained when the system runs off-line. Due to time constraints it was however not possible to implement the Bachmann controller in the loop. This is the only objective that has not been achieved.
A step by step method to develop a WFC for the active power part has been presented in this work and is summarized in Figure 7.1.

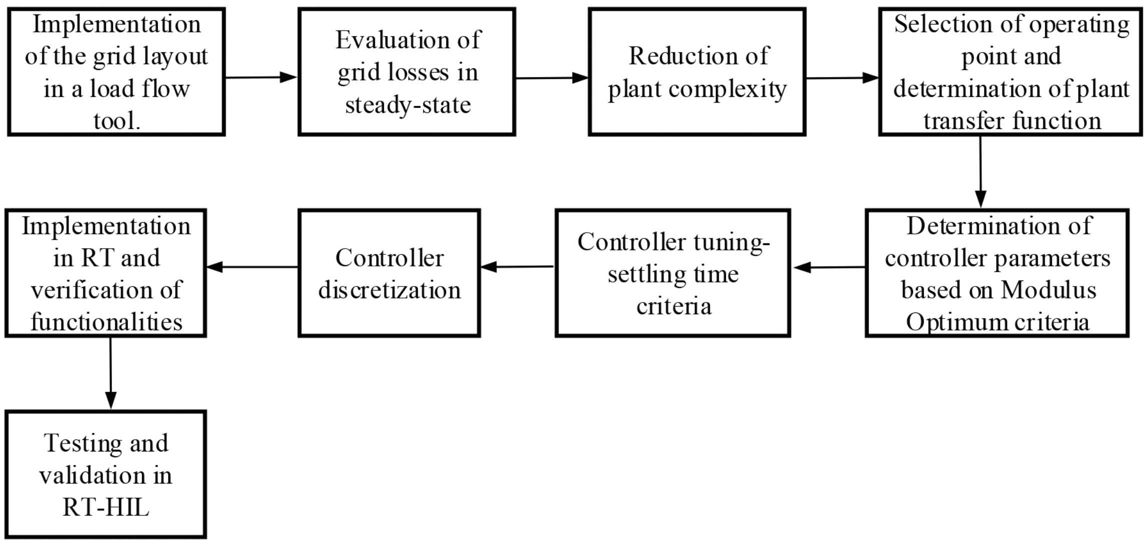

Figure 7.1. Steps needed to develop the active power control of a WF.

8 Future Work

Even though the majority of the goals, which were expressed in the begging of the project were achieved, there is still some work which has not been completed and there are also some topics which need further research. The following issues should therefore be addressed as a continuation of this work:

- Implementation of the Bachmann controller in the loop and evaluation of the influence of communication delays between the controller and the assets.
- Merge the active power-frequency control and reactive power-voltage control to obtain a complete controller and assess the behaviour during unusual operating conditions, such as unbalance or faults.
- Investigate optimized dispatch strategies to reduce active power loss, improve life time of the WF or to fulfil another goal.

Bibliography

[1] E. W. E. Association, "The european offshore wind industry -key trends and statistics 2015," European Wind Energy Association (EWEA), Tech. Rep., February 2016.

[2] J. M. Garcia, "Voltage control in wind power plants with doubly fed generatos," Ph.D. dissertation, Aalborg University, 2010.

[3] L. Petersen and F. Kryezi, "Wind power plant control optimisation with embedded application of wind turbines and statcoms," Master's thesis, Aalborg University, 2015.

[4] J. N. Jiang, C. Y. Tang, and R. G. Ramakumar, *Control and Operation of Grid-Connected Wind Farms; Major Issues, Contemporary Solutions and Open Challenges.* Springer, 2016.

[5] Energinet.dk, "Technical regulation 3.2.5 for wind power plants above 11 kw," Energinet.dk, Tech. Rep., 2016.

[6] T. Knudsen, T. Bak, and M. Svenstrup, "Survey of wind farm control—power and fatigue optimization," *Wind Energy*, vol. 18, pp. 1333–1351, May 2014.

[7] V. Spudic, M. Jelavic, M. Baotic, M. Vasak, and N. Peric, "Distributed control of large-scale offshore wind farms(aeolus)-deliverable 3.3:reconfigurable control extension," University of Zagreb Faculty of Electrical Engineering and Computing Department of Control and Computer Engineering, Tech. Rep., 2008.

[8] H. Saadat, *Power System Analysis.* Mcgraw-Hill College, 1998.

[9] P. Sørensen, A. D. Hansen, K. Thomsen, ThomasBuhl, P. E. Morthorst, L. H. Nielsen, F. Iov, F. Blaabjerg, H. A. Nielsen, H. Madsen, and M. H. Donovan, "Operation and control of large windturbines and wind farms - final report," Risø National Laboratory, Roskilde, Denmark, Tech. Rep., 2005.

[10] V. Spudic, M. Jelavic, M. Baotic, and N. Peric, "Distributed control of large-scale offshore wind farms(aeolus)-deliverable 5.6: Assessment and validation of relative performance of control strategies," University of Zagreb Faculty of Electrical Engineering and Computing Department of Control and Computer Engineering, Tech. Rep., 2008.

[11] X. Guan and G. M. van der Molen, "Distributed control of large-scale offshore wind farms(aeolus)-deliverable 3.1: Control strategy review and specification," AEOLUS, Tech. Rep., 2009.

[12] F. Ebrahimi, A. Khayatiyan, and E. Farjah, "A novel optimizing power control strategy for centralized wind farm control system," *Renewable Energy*, vol. 86, pp. 399–408, August 2016.

[13] A. D. Hansen, P. Sørensen, F. Iov, and F. Blaabjerg, "Centralised power control of wind farm with doubly fed induction generators," *Renewable Energy*, vol. 31, pp. 935–951, 2006.

[14] R. G. de Almeida, E. D. Castronuovo, and J. A. P. Lopes, "Optimum generation control in wind parks when carrying out system operator requests," *IEEE Transactions on Power Systems*, vol. 21, no. 2, pp. 718–725, May 2006.

[15] L. Petersen, F. Iov, A. D. Hansen, and M. Altin, "Voltage control support and coordination between renewable generation plants in mv distribution systems," *15th Wind INtegration Workshop*, 2016.

[16] C. Tang, M. Pathmanathan, W. Soong, and N. Ertugrul, "Effects of inertia on dynamic performance of wind turbines," in *2008 Australasian Universities Power Engineering Conference (AUPEC'08)*, 2008, pp. 1–6.

[17] "General specification: V112–3.0 mw 50/60 hz," Vestas Wind Systems A/S, Tech. Rep., 2010.

[18] A. Honrubia-Escribano, F. Jiménez-Buendía, E. Gómez-Lázaro, and J. Fortmann, "Validation of generic models for variable speed operation wind turbines following the recent guidelines issued by iec 61400-27," *Energies*, vol. 9, 2016.

[19] T. N. Preda, K. Uhlen, D. E. Nordgård, and T. Toftevaag, "External grid representation for assessing fault ride through capabilities of distributed generation units," *IEEE*, 2012, 3rd IEEE PES Innovative Smart Grid Technologies Europe (ISGT Europe), Berlin.

[20] C. Ionita and R. Celiloglu, "Coordinated control and grid support of renewable generation plants," Aalborg University, Tech. Rep., 2016, 8th Semester Project.

[21] C. L. Phillips and J. M. Parr, *Feedback Control Systems*, 5th ed. Pearson, 2013.

[22] D. Schröder., "Elektrische antriebe-regelung von antriebssystemen," *Springer Science & Business Media*, vol. 10, 2009.

[23] C. Bajracharya, M. Molinas, J. A. Suul, and T. M. Undeland, "Understanding of tuning techniques of converter controllers for vsc-hvdc," *Nordic Workshop on Power and Industrial Electronics(NORPIE)*, 2008.

[24] K. J. Aström and R. M. Murray, *Feedback Systems- An Introduction for Scientists and Engineers.* PRINCETON UNIVERSITY PRESS, 2009.

[25] J. Feng and W. Z. Shen, "Modelling wind for wind farm layout optimization using joint distribution of wind speed and wind direction," *Energies*, vol. 8, pp. 3075–3092, 2015.

[26] T. Gocmen and G. Giebel, “Estimation of turbulence intensity using rotor effective wind speed in lillgrund and horns rev-i offshore wind farms,” *Renewable Energy*, 2016.

[27] E. V. Laursen, “Weather statistics for airports, 2003-2012 denmark and faroe islands,” DMI, Tech. Rep., 2012.

[28] F. Iov, A. D. Hansen, P. Sørensen, and Fre, “Wind turbine blockset in matlab/simulink- general overview and description of the models,” Aalborg University, Tech. Rep., 2004.

[29] F. D. Bianchi, H. D. Battista, and R. J. Mantz, *Wind Turbine Control Systems*. Springer, 2006.

[30] J. Marcos, I. de la Parra, M. García, and L. Marroyo, “Control strategies to smooth short-term power fluctuations in large photovoltaic plants using battery storage systems,” *Energies*, vol. 7, pp. 6593–6619, 2014.

[31] L. Petersen and F. Iov, “Practical considerations regarding implementation of wind power applications into real-time hardware-in-the-loop framework,” in *NEIS Conference*, 2016, pp. 61–66.